Dynamics of oxygen unloading from sickle erythrocytes

Vinod B. Makhijani,* Giles R. Cokelet,‡ and Alfred Clark, Jr.*
*Department of Mechanical Engineering, University of Rochester, Rochester, New York 14627; and ‡Department of Biophysics, University of Rochester, Rochester, New York 14642 USA

ABSTRACT The objective of this work is to theoretically model oxygen unloading in sickle red cells. This has been done by combining into a single model diffusive transport mechanisms, which have been well-studied for normal red cells, and the hemoglobin polymerization process, which has previously been studied for deoxyhemoglobin-S solutions and sickle cells in near-equilibrium situations. The resulting model equations allow us to study the important processes of oxygen delivery and polymerization simultaneously. The equations have been solved numerically by a finite-difference technique. The oxygen unloading curve for sickle erythrocytes is biphasic in nature. The rate of unloading depends in a complicated way on (*a*) the kinetics of hemoglobin S polymerization, (*b*) the kinetics of hemoglobin deoxygenation, and (*c*) the diffusive transport of both free oxygen and oxy-hemoglobin. These processes interact. For example, the hemoglobin S polymer interferes with the transport of both free oxygen and unpolymerized oxy-hemoglobin, and this is accounted for in the model by diffusivities which depend on the polymer and solution hemoglobin concentration. Other parameters which influence the interaction of these processes are the concentration of 2,3-diphosphoglycerate and total hemoglobin concentration. By comparing our model predictions for oxygen unloading with simpler predictions based on equilibrium oxygen affinities, we conclude that the relative rate of oxygen unloading of cells with different physical properties cannot be correctly predicted from the equilibrium affinities. To describe the unloading process, a kinetic calculation of the sort we give here is required.

INTRODUCTION

Mathematical models of oxygen transport in red cells have been presented by Moll (1969), Kutchai (1970), Sheth (1979), Sheth and Hellums (1980), Baxley and Hellums (1983), Federspiel (1983), Clark et al. (1985), and Lemon et al. (1987). The processes governing the rate of oxygen transport within erythrocytes are the deoxygenation of, hemoglobin and the diffusion of oxygen and hemoglobin. The processes for sickle erythrocytes are complicated by the reduction of the solubility of sickle hemoglobin, HbS, on deoxygenation (Singer and Singer, 1953). For concentrations beyond a critical solubility, HbS tends to polymerize. The polymer binds oxygen noncooperatively and with a lower affinity than the deoxyhemoglobin molecules in solution (Sunshine et al., 1982).

Minton (1974, 1975, 1976, 1977) proposed a thermodynamic model which adequately explained physical properties such as the effect of temperature and concentration on sickle hemoglobin gelation under equilibrium conditions. Sunshine et al. (1982) reproduced the equilibrium oxygen dissociation curve theoretically using a two phase model for a hemoglobin gel (solution + polymer).

Ferrone et al. (1985*a*) studied polymer formation in HbS solutions at physiological hemoglobin concentrations using the laser photolysis technique. They used an argon ion laser to photodissociate a carbon monoxide complex of hemoglobin S and monitor polymer formation from the change in light scattering. They also proposed a theoretical model which incorporated kinetic and thermodynamic parameters of the double nucleation mechanism (Ferrone et al., 1980; Bishop and Ferrone, 1984; Ferrone et al., 1985*b*). Their model reproduced polymerization kinetics in the first 15% of the polymer growth curve for a deoxyhemoglobin S solution (zero fractional oxygen saturation). The laser photolysis experiments gave considerable insight into the nucleation and growth mechanisms of the polymerization process. Their data, however, were not relevant to physiological situations where polymerization is induced by spontaneous deoxygenation of erythrocytes in the microcirculation and where the kinetics of intracellular polymer formation depend on the rate of deoxygenation.

Intracellular sickle hemoglobin gelation was studied by Noguchi et al. (1980) in erythrocyte samples undergoing very slow (~50 h) but spontaneous deoxygenation. They used natural abundance ^{13}C NMR spectroscopy to quantitate the polymer fraction in sickle cells at different oxygen saturations. Their experimental data closely agreed with their theoretical estimates of polymer fractions at equilibrium which indicated the existence of near equilibrium conditions in the erythrocytes during their extremely slow deoxygenation experiments. However, it was not

0006-3495/90/10/1025/28 $2.00

clear whether such equilibrium conditions existed in vivo in sickle red cells undergoing deoxygenation at a much faster rate (~1 s) in the microcirculation.

Stathopoulous et al. (1987) made an attempt to model the dynamic process of sickle erythrocyte deoxygenation in the microcirculation. They presented theoretical results for oxygen transport by a sickle cell suspension flowing down a capillary. Their theoretical model accounted for hemoglobin diffusion and nonlinear deoxygenation kinetics based on the oxygen-HbS equilibrium curve. They, however, didn't incorporate the effect of polymerization on the deoxy HbS concentration or on the free and facilitated diffusion of oxygen. Moreover, their equilibrium curve data for sickle blood, used in the modeling of deoxygenation kinetics, only reflected the effect of polymer on the oxygen affinity of sickle hemoglobin during equilibrium conditions. The various processes occurring in a sickle erythrocyte during deoxygenation have substantially different kinetic rates; hence, such a quasi-equilibrium approach to modeling oxygen transport from sickle red cells would fail to adequately represent, under many conditions, the dynamics of sickle erythrocyte deoxygenation.

Sickle red cells have an elevated intracellular 2,3-DPG (diphosphoglycerate) concentration (Charache et al., 1970) which influences the oxygen affinity of hemoglobin. 2,3-DPG is known to decrease the oxygen affinity of normal adult hemoglobin (HbA) by binding specifically to deoxyhemoglobin and stabilizing the tense, deoxy conformation (Arnone, 1972). The effect of elevated molar ratios of 2,3-DPG to hemoglobin (Hb) on the kinetics of deoxygenation and the oxygen equilibrium curve for normal human blood has been studied in the past (Salhany et al., 1970; Bauer et al., 1973; Samaja and Winslow, 1979; Samaja et al., 1981). An increase in 2,3-DPG levels causes a right shift in the oxygen dissociation curve for normal hemoglobin. Unpolymerized HbS in solution behaves like normal hemoglobin in terms of its oxygen affinity (Pennelly and Noble, 1978). It is not surprising, therefore, that higher levels of 2,3-DPG in sickle red cells contribute to the decreased oxygen affinity in sickle cell anemia (Charache et al., 1970).

HbS polymerization occurs when hemoglobin S is deoxygenated and, hence, a compound which alters the oxygen affinity of hemoglobin S is likely to affect the degree of sickling at a given partial pressure of oxygen. Jensen et al. (1973) studied the effect of increased intracellular 2,3-DPG concentrations on the phenomenon of sickling at equilibrium conditions and concluded that it enhanced HbS aggregation and, consequently, the formation of low O_2 affinity polymer at a given P_{O_2}. Thus, the intraerythrocyte organic phosphate influences the oxygen affinity of sickle hemoglobin directly (by stabilizing deoxy HbS) and indirectly (by influencing the polymer concentration at a given P_{O_2}). No previous attempts have been made to isolate these two effects at equilibrium conditions or compare their contribution to the dynamic process of oxygen unloading in sickle erythrocytes.

Zarkowsky and Hochmuth (1977) studied the effect of 2,3-DPG concentrations on the kinetics of sickling in erythrocytes subjected to sudden deoxygenation with sodium dithionite. Their data showed that a reduction in intracellular 2,3-DPG concentration significantly increased the time interval between complete deoxygenation and the onset of morphologic deformation (sickling time) in sickle erythrocytes. The sickling time in their experiments, however, was essentially independent of the kinetics of hemoglobin desaturation, and the large alteration in sickling time was probably due to the influence of 2,3-DPG concentration on deoxy HbS solubility (Poillon et al., 1986). The effect of elevated 2,3-DPG/Hb molar ratios on the kinetics of intracellular polymerization due to their effect on the rate of oxygen unloading has not been investigated yet.

Chien et al. (1970) showed that any red cell population in sickle cell anemia displayed a wide spectrum of intracellular HbS concentrations with the mean corpuscular hemoglobin concentration (MCHC) ranging from 0.2 to 0.5 g/cc. Seakins et al. (1973) studied the effect of erythrocyte HbS concentration on the oxygen affinity of hemoglobin at equilibrium conditions and compared it to the effect of the diphosphoglycerate-hemoglobin molar ratio. They found the affinity of HbS lowered when they did the analysis for samples with a higher MCHC and lower molar ratio. This led them to conclude that HbS concentration played a greater part than the intracellular 2,3-DPG levels in lowering the oxygen affinity of blood in sickle cell anemia (due to its influence on the formation of low affinity polymer). This analysis again was at equilibrium conditions and gave no information on the relative effects of these two parameters on the rates of oxygen unloading and HbS polymerization in sickle red cells.

A theoretical model, which includes (*a*) diffusive transport of free (unpolymerized) oxygenated and deoxygenated HbS, (*b*) diffusive transport of free oxygen, and (*c*) the kinetics of deoxygenation and polymerization of HbS, is developed for the simulation of oxygen delivery from sickle red cells and intracellular polymerization in the microcirculation. The oxygen unloading curves for normal and sickle red cells, with physiological intracellular concentrations of 2,3-DPG and the same mean corpuscular hemoglobin concentration (MCHC), are compared using the same external extraction environment. The effects of 2,3-DPG/Hb molar ratio, intraerythrocyte hemoglobin concentration and boundary P_{O_2} on the mechanisms influencing the rate of oxygen unloading and HbS polymerization in sickle erythrocytes are also studied. Finally, to establish the relevance of oxygen affinity

analysis done at equilibrium conditions to the actual process of oxygen delivery, the oxygen unloading curves are simulated for the same parameter values used by Seakins et al. (1973) in their study on oxygen affinity.

GLOSSARY

Principal symbols

(The concentration and reaction rates are per unit volume of cell and fluxes per unit area of cell unless indicated otherwise.)

B	Bunsen solubility coefficient for oxygen
B_{H_2O}	Bunsen solubility coefficient for water
C_H	density of unaggregated monomer (g/cc monomer)
C_p	density of polymer (g/cc polymer)
C_{sol}	HbS solubility (g/cc solution)
$C_{sol,0}$	deoxy HbS solubility (g/cc solution)
C_t	total hemoglobin concentration
D_k	diffusivity of species "k" in the solution
F_k	flux for species "k"
$[Hb]$	concentration of free hemoglobin in the solution (g/cc solution)
K	dissociation rate constant for deoxygenation
K_+	reaction rate constant for addition of monomer to nuclei/polymer
N_k	molar concentrations of unpolymerized species "k"
N_{50}	molar concentration of oxygen at equilibrium at 50% saturation
P_k	partial pressure of species "k" in solution
P_{50}	partial pressure of oxygen at equilibrium at 50% solution fractional oxygen saturation
$(P_{50})_t$	partial pressure of oxygen at equilibrium at 50% total fractional oxygen saturation
S	degree of supersaturation of deoxy HbS monomer
T	temperature
Y_p	polymer phase fractional oxygen saturation of hemoglobin
Y_s	solution phase fractional oxygen saturation of hemoglobin
Y_t	total fractional oxygen saturation of hemoglobin
Γ_1	reaction rate for deoxygenation
Γ_2	reaction rate for polymerization
a	half cell width
i^*	size of critical homogenous nucleus
j^*	size of critical heterogenous nucleus
n	dimensionless exponent in the Hill equation
n_H	molar concentration of polymerized deoxy monomer
n_H^*	molar concentration of polymer ends
n_{H,j^*}^*	molar concentration of heterogenous nuclei
pH_e	plasma pH
pH_i	pH of solution in the red cell
t	time
t_d	delay time, defined as the time that elapses, during deoxygenation, between the formation of supersaturation and the time when the cell-averaged polymer concentration reaches a specified level
ts	time scale
v_k	volume fraction of phase "k" in the cell
v_{eff}	area fraction of the cell available for diffusion
x_k	mole fraction of phase "k" in the cell
x	spatial distance along width of the cell
γ	monomer activity coefficient
γ_{sol}	activity coefficient of soluble part of the monomer
γ_{i^*+1}	activity coefficient of activated complex (i.e., homogenous nucleus +1 monomer)
$\gamma_{i^*}\, n_{H,i^*}^*$	activity of homogeneous nuclei in millimolar units
ϕ	area fraction of polymerized monomer surface available for heterogenous nucleation

Subscripts

CO_2	carbon dioxide
H	deoxyhemoglobin
HO	oxyhemoglobin
O, O_2	oxygen
avg	spatially averaged
cr	critical
f	free (unpolymerized)
h	higher molar ratio of 1.5
i	initial
l	lower molar ratio of 1
s	solution
sol	soluble
sup	supersaturated
p	polymer
w	cell wall (boundary)

Superscripts

	nondimensional quantities
~	quantities per unit volume of solution
1, 2, 3	for hemoglobin densities of 0.35, 0.34, and 0.33 g/cc, respectively
A	for a hemoglobin density of 0.324 g/cc
B	for a hemoglobin density of 0.362 g/cc

MECHANISMS GOVERNING OXYGEN UNLOADING RATES

Oxygen moves by both free and facilitated diffusion from the center of the red cell to the cell membrane in normal erythrocytes during the unloading process. Facilitated diffusion results from the movement of oxyhemoglobin, HbO_2, toward the cell wall. This oxyhemoglobin undergoes simultaneous diffusion and deoxygenation, resulting in free O_2 and deoxy HbA. The unbound oxygen diffuses out of the cell and deoxy HbA diffuses back toward the cell center. Local concentrations of the normal adult hemoglobin, HbA (oxy + deoxy), remain constant during the process.

Sickle red cells unload O_2 in a manner similar to that of normal red cells until the soluble HbS concentration

becomes lower than the total HbS concentration. Polymerization begins after a characteristic latent period and acts as a "sink" for the deoxy HbS molecules (see Fig. 1). The deoxy HbS molecules incorporated in the polymer are unable to diffuse toward the center of the cell because of the large size of the aggregates.

Polymerization affects the deoxygenation reaction by "removing" deoxy HbS from the solution. (Because the polymer binds oxygen so weakly, the ooygen removal from the solution by polymerization is generally negligible.) Diffusion is also affected because (*a*) the polymer is a barrier to the diffusion of O_2 and the free oxy and deoxy HbS components, and, (*b*) polymerization alters the solution hemoglobin concentration and, consequently, the diffusivities of oxygen and hemoglobin, and their concentration gradients, in the solution. These are the direct effects of polymerization. There are certain other indirect effects which, due to the extremely nonlinear interdependence of the three mechanisms (deoxygenation, diffusion, and polymerization), cannot be visualized without actually solving the transport equations. These will be dealt with later. However, it is obvious at this point that the HbS "sink" results in a diffusive redistribution of local HbS (free oxy, deoxy, and polymer) concentrations.

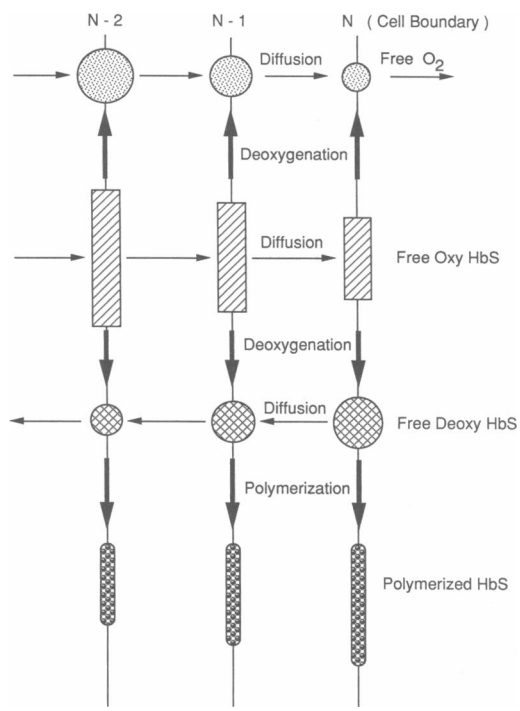

FIGURE 1 A schematic for the processes and conditions at three locations inside a sickle erythrocyte during oxygen removal. The column on the right shows conditions next to the cell wall; the other two columns represent two interior locations progressively nearer the cell center. Each row represents a chemical species in the cell; the symbol sizes indicate the relative local concentration of a species at different positions in the cell. The horizontal and vertical arrows represent physical diffusion and the chemical reactions, respectively.

MODEL FOR OXYGEN DELIVERY

Basic assumptions

The red cell, as a first approximation, is modeled as a one-dimensional slab of thickness $2a$. This choice of slab geometry has been used in previous models for O_2 transport in normal red cells (Moll, 1969; Kutchai, 1970; Sheth and Hellums, 1980; Clark et al., 1985). Oxygen delivery from the sides of the sickle red cells can be modeled using this kind of a geometry. Transport from the edges of the red cell and the red cell curvature are ignored. We use a typical half width value of $a = 1$ μm in our model.

HbS is assumed to exist in two phases: free Hb in solution (T-state and R-state) and polymerized Hb (T-state molecules only). This is based on the extension of the two state allosteric model (Monod et al., 1965) to the gelation of HbS (Sunshine et al., 1982). The amount of oxygen bound to the polymer is assumed negligible. The plasma pH outside the cell, pH_e, is assumed to be constant. The P_{CO_2} is taken as 40 Torr and the physical and kinetic constants are obtained at a temperature of 35°C.

Transport equations

The transport equations are derived from mass balances for the four species: free oxygen, free oxyhemoglobin and deoxyhemoglobin, and polymerized deoxyhemoglobin. Processes entering the mass balance are, in general, convection, diffusion, and chemical reactions. We neglect convective effects of internal flow within the red cells in the present work. Then we have

$$\frac{\partial N_O}{\partial t} = -\nabla \cdot \boldsymbol{F}_O - \Gamma_1 \tag{1}$$

$$\frac{\partial N_{HO}}{\partial t} = -\nabla \cdot \boldsymbol{F}_{HO} + \Gamma_1 \tag{2}$$

$$\frac{\partial N_H}{\partial t} = -\nabla \cdot \boldsymbol{F}_H - \Gamma_1 - \Gamma_2 \tag{3}$$

$$\frac{\partial n_H}{\partial t} = \Gamma_2, \tag{4}$$

where $\boldsymbol{F}_O$, $\boldsymbol{F}_{HO}$, and $\boldsymbol{F}_H$ are the fluxes for oxygen, oxyhemoglobin, and deoxyhemoglobin, respectively. The hemoglobin (molecular weight 64 kD) and oxygen concen-

trations are in millimolars. The concentrations and reaction rates are per unit volume of the cell. The fluxes are per unit area.

The difficulty with the transport equations comes when we attempt to supply explicit expressions for the fluxes and reaction rates. In some cases, these functions are more easily estimated in terms of quantities per unit volume of solution than per total unit volume (of cell). Both these descriptions are closely connected with alternate viewpoints based on the description of the system. During the initial stages of the unloading process, before the initiation of polymerization, these two definitions coincide. The problem arises after the deoxyhemoglobin monomers in the solution start aggregating.

We define the system, in general, as consisting of polymer and hemoglobin solution. The volume fractions, in the cell, of the solution and polymer are v_s and $v_p = 1 - v_s$, respectively. We denote quantities per unit volume of the solution by $\sim$. Then concentrations and reaction rates per unit volume of the solution are given by $\tilde{N} = N/v_s$ and $\tilde{\Gamma} = \Gamma/v_s$. Finally, we define fluxes per unit area of solution as $\tilde{F}$. If we assume the impenetrable polymer to be uniformly interspersed in a unit volume of the cell, then the area fraction of the cell available for diffusion decreases by a factor which depends on the size, shape, and distribution of the barriers. For dilute barriers, this factor depends only on their volume fraction and is given by (Crank, 1975):

$$v_{eff} = \frac{1 - v_p}{1 + (v_p/2)} = \frac{2v_s}{3 - v_s}. \tag{5}$$

Taking this area reduction into account, we have $\tilde{F} = F/v_{eff}$. We can rewrite the transport equations in terms of these quantities. The general form is

$$\frac{\partial}{\partial t}(v_s\tilde{N}) = -\nabla \cdot (v_{eff}\tilde{F}) + v_s\tilde{\Gamma} \tag{6a}$$

or

$$\frac{\partial \tilde{N}}{\partial t} = -\frac{1}{v_s}\nabla \cdot (v_{eff}\tilde{F}) + \tilde{\Gamma} - \frac{\tilde{N}}{v_s}\frac{\partial v_s}{\partial t}. \tag{6b}$$

We now look at the individual fluxes and reaction rates.

Kinetics of deoxygenation

Unpolymerized HbS solution has the same oxygen affinity as HbA (Pennelly and Noble, 1978) for a given Hb concentration and 2,3-DPG/Hb molar ratio. We assume that the deoxygenation kinetics for unpolymerized HbS are similar to that for HbA. The four step reaction scheme is represented by the simpler one step approximation used by many previous authors

$$Hb_f + O_2 \leftrightarrow Hb_fO_2, \tag{7}$$

where Hb_f represents free deoxy HbS. We adopt the kinetic expression from Clark et al. (1985)

$$\tilde{\Gamma}_1 = K\left[\tilde{N}_H\left(\frac{\tilde{N}_O}{\tilde{N}_{50}}\right)^n - \tilde{N}_{HO}\right], \tag{8}$$

where $\tilde{\Gamma}_1$ is the reaction rate for Eq. 7 based on a unit volume of the solution. The molar concentrations, $\tilde{N}_H$, $\tilde{N}_{HO}$, $\tilde{N}_O$, and $\tilde{N}_{50}$ are also expressed in terms of a unit volume of the solution. Because the solution phase in the cell behaves like normal hemoglobin, $\tilde{N}_O = BP_{O_2}$ for an oxygen partial pressure of P_{O_2} and solubility B. Although the solubility of oxygen is altered by intracellular polymer formation (this effect is discussed elsewhere), we assume the effect to be negligible when $P_{O_2} \geq P_{50}$. The oxygen concentration at 50% solution fractional saturation, $\tilde{N}_{50}$, therefore, is equal to BP_{50}. $\tilde{\Gamma}_1 = 0$ gives the equilibrium oxygen dissociation curve fit well by the Hill equation. The reaction rate based on a unit volume of the system is given by

$$\Gamma_1 = K\left[N_H\left(\frac{\tilde{N}_O}{\tilde{N}_{50}}\right)^n - N_{HO}\right]. \tag{9}$$

Kinetics of polymerization

The polymerization process can be represented by a simple reaction

$$Hb_f \leftrightarrow Hb_p, \tag{10}$$

where completely deoxygenated unpolymerized HbS monomers form polymerized Hb aggregates with a reaction rate of Γ_2. The polymerization kinetics of HbS in solution were modeled theoretically for the initial part of the process (<15% polymerization) by Ferrone et al., (1985*b*) at zero fractional oxygen saturation. Polymerization inside red cells proceeds by the same nucleation and growth mechanisms as in deoxy HbS solutions (Coletta et al., 1982). Goldberg et al. (1981, 1982) had previously demonstrated that intracellular sickling isn't significantly enhanced by the existence of possible nucleation sites on a red cell membrane. We, therefore, used the model by Ferrone et al. (1985*b*) to simulate in vivo HbS polymerization by extending it to nonzero fractional saturations.

The rate equations developed by Ferrone et al. (1985*b*) can be written as

$$\frac{\partial n_H^*}{\partial t} = K_+(\gamma N_H)\left[n_{H,j^*}^* + \left(\frac{\gamma_{i^*} n_{H,i^*}^*}{\gamma_{i^*+1}}\right)\right] \tag{11}$$

$$\Gamma_2 = K_+[(\gamma N_H) - (\gamma_{sol} N_{H,sol})]\, n_H^*, \tag{12}$$

where, at 35°C (see Appendix 1),

$$(\gamma_{i^*} n^*_{H,i^*}) = (\gamma_{sol} N_{H,sol}) \exp [15.6087 \cdot \ln (\ln S) - 22.7081] \quad (13)$$

$$n^*_{H,j^*} = \phi n_H \exp [16.6087 \ln (\ln S) - 22.509] \quad S < 3.5099 \quad (14)$$

$$= \phi n_H \exp [13.2278 \ln S - 35.3375] \quad 3.5099 \le S \le 4.4034 \quad (15)$$

$$= \phi n_H \exp [2.5419 \ln (\ln S - 1.2902) - 11.5362] \quad S > 4.4034 \quad (16)$$

$$S = \frac{\gamma N_H}{\gamma_{sol} N_{H,sol}}. \quad (17)$$

For convenience, all concentrations and the reaction rate involved in the polymerization kinetics are expressed per unit total volume. $N_{H,sol}$ is the concentration of soluble deoxyhemoglobin. n_H is the molar concentration of polymerized monomer (moles of deoxy monomer in the polymer per unit total volume) and S represents the supersaturation of the monomer. The values of ϕ and K_+ at 35°C are 5.2481×10^{-4} and 3.4674×10^3 $mM^{-1}s^{-1}$, respectively.

Eqs. 11 and 12 represent nucleation and growth for the polymerization process (see Fig. 2), respectively. Ferrone et al. (1985*b*) assumed that the addition of a single deoxy HbS monomer to either a homogenous nucleus (molar concentration = n^*_{H,i^*}) or a heterogenous nucleus (molar concentration = n^*_{H,j^*}) results in the formation of a polymer. The nucleation process was taken to be effectively irreversible and hence, there is no back reaction term in Eq. 11. This process results in an increase in the concentration of polymer ends, n^*_H. Here, solution nonideality, a prominent feature of sickle hemoglobin polymerization, plays an important role in the kinetics of the process.

At concentrations required for polymerization, the protein molecules occupy a significant fraction of the solution volume and hence, the total solution volume is not available to the HbS monomer and aggregates. The excluded volume effect shows up as large activity coefficients in the kinetic equations where activities are used instead of molar concentrations. (Activity coefficients were not used earlier in the discussion on the kinetics of deoxygenation as published data on the dissociation rate constant, K, are based on molar concentrations, rather than activities, of O_2 and the Hb components.) Although oxyhemoglobin S molecules are a nonpolymerizing species and do not have any specific involvement in the process of gelation, they exert their influence by increasing the activity coefficients of the deoxy HbS monomer (γ, γ_{sol}) and the activated complex (γ_{i^*+1}). Behe and Englander (1978) had shown that the addition of a foreign protein (having the same size and shape as HbS) in an HbS solution had the same effect on the HbS activity coefficient as the presence of HbS molecules itself. Eaton and Hofrichter (1978) used this rationale to compute, to a first approximation, the activity coefficients of the deoxy HbS monomer and the activated complex in solutions of hemoglobin S partially saturated with carbon monoxide. Adopting a similar approach, we get activity coefficients of the form $\gamma = f_1(N_H + N_{HO})$, $\gamma_{sol} = f_i(N_{H,sol} + N_{HO})$, and $\gamma_{i^*+1} = f_2(N_H, N_{H,sol}, N_{HO})$. The functions f_1 and f_2 are given in Appendix 2.

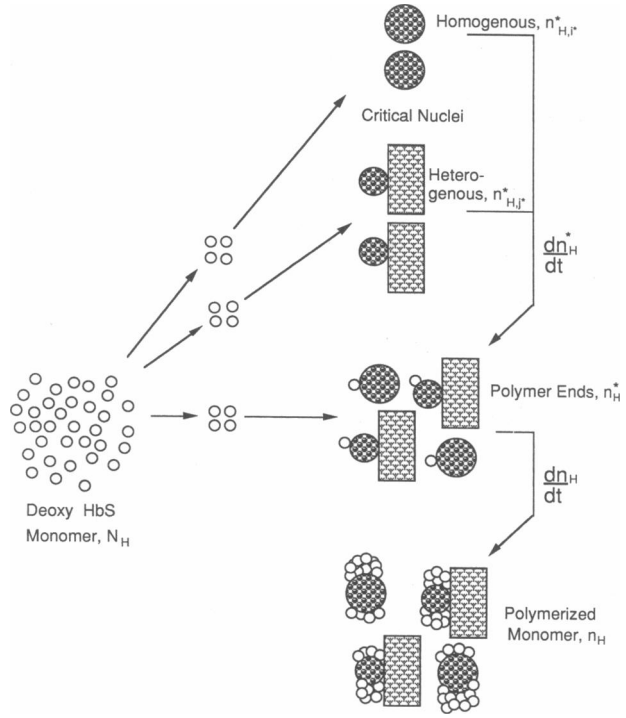

FIGURE 2 A schematic representation of the mechanisms of deoxy HbS polymerization (i.e., nucleation and growth). The small open circles represent deoxyhemoglobin monomers which can react to form nuclei (*larger shaded circles*) in the solution (homogenous nucleation) or on already existing polymer (heterogenous nucleation), or which can contribute to the growth of existing polymer (*shaded rectangles*).

The activity of the homogenous nuclei, $\gamma_{i^*} n^*_{H,i^*}$, is divided by the activity coefficient of the activated complex to obtain the rate of increase of concentration of the polymer ends due to homogenous nucleation. The heterogenous nuclei are attached to the polymer, treated thermodynamically as a crystal, and hence the activity coefficients for the j*-mer and j* + 1-mer cancel out.

Monomer depletion from the HbS solution occurs due to the formation of polymer ends and the addition of monomer to existing polymer ends. Although polymer growth is accompanied by the alignment of polymer fibers (Hofrichter et al., 1976), initial polymer domains are largely unaligned and form as entangled polymer masses (Basak et al., 1988). Because the model is valid only for

the initial part of the polymerization process, we neglect directionality effects of polymer alignment on the process of monomer depletion (and on the diffusive fluxes).

The entire polymerization kinetics (Eqs. 11–17) are governed by the relative rate of change of N_H and $N_{H,sol}$ or, effectively, the rate of change of the degree of supersaturation of the HbS solution in the cell. The process of polymer growth is initiated by the nucleation mechanism only after the HbS solubility, C_{sol}, falls below the total HbS concentration in the cell, C_t, resulting in supersaturated hemoglobin solution. HbS solubility increases and decreases monotonically with increasing and decreasing fractional saturation of free hemoglobin respectively (Sunshine et al., 1982). Therefore, a deoxy HbS solution formed by laser photolysis has minimal HbS solubility ($C_{sol,0}$), resulting in maximum supersaturation for a given HbS concentration. The elapsed time from the photolysis to the time when a physical change in the HbS solution is detectable (a so-called delay time, t_d) is inversely proportional to the supersaturation for a fixed C_t (Hofrichter et al., 1976), and is therefore minimal for such conditions. The degree of supersaturation decreases as polymerization proceeds and eventually vanishes on completion of the aggregation process.

Polymerization kinetics for a sickle cell unloading O_2 differ from the photolysis case above in that the starting point for nucleation is infinitesimal supersaturation. As the cell unloads oxygen, the solution fractional saturation, Y_s, and hence solubility, C_{sol}, decreases. This results in an initial gradual increase in the extent of supersaturation of the HbS solution during the latent period which tends to accelerate the nucleation process and effectively decrease the delay time. Once the delay period is overcome, the increase in the supersaturation is opposed by a negative tendency resulting from an accelerated rate of monomer aggregation. If the cell unloads all its oxygen during the delay period, maximum supersaturation is at the point where $Y_s = 0$. If, however, the latent period elapses before the cell has fully unloaded, S reaches a maximum value at some intermediate Y_s. Beyond this point, S decreases until polymerization is complete. In this case, the polymer interferes with the unloading of the remaining O_2 from the sickle cell. The complexity of this oxygen delivery process arises from the fact that beyond a threshold point, the rate of O_2 unloading not only determines the rate of decrease of O_2 and HbO_2 in the cell but also influences the degree of diffusive obstruction encountered by these diminishing components.

Fluxes

We first need to define our system inside the cell before we estimate the fluxes of the various components. At high P_{O_2}, when the polymer concentration is small, the small clumps of polymer can be treated as large molecules, and the interior of the sickle cell is essentially a (nonideal) solution. At the opposite extreme, when the polymer concentration is high, the polymer structure can be like a rigid, macroscopic matrix, and then the interior of the cell is like a heterogenous material, perhaps even like a porous medium. Traditionally these qualitatively different situations are analyzed using totally different kinds of models. It is very difficult to find a model which can handle these two extremes and the continuous variation between them. The estimation of the diffusive flux in a partially polymerized cell is very difficult. In the worst case, there is considerable polymer present in a concentration which varies with position. In principle, we have to deal with diffusion in a heterogenous material which is not statistically homogenous, and in which the heterogenities are not dilute.

We take a much simpler and cruder approach and assume that the fluxes in the solution phase are normal. This assumption is quite reasonable because polymer concentrations in our model are quite small. Thus the flux per unit area of solution is equal to the normal diffusivity times the gradient of concentration per unit volume of the solution. The flux equations are then

$$\tilde{F}_O = -D_O \nabla \tilde{N}_O \tag{18}$$

$$\tilde{F}_H = -D_H \nabla \tilde{N}_H \tag{19}$$

$$\tilde{F}_{HO} = -D_{HO} \nabla \tilde{N}_{HO}. \tag{20}$$

The fluxes per unit area of the cell are obtained by multiplying Eqs. 18–20 by v_{eff}. The hemoglobin molecule is much larger than the oxygen molecule and, hence, we can take $D_{HO} = D_H$ with a high degree of accuracy.

We express the molar concentrations as a function of x and t. Taking all the assumptions into account, the transport equations, Eqs. 1–3, in the final form are (see Appendix 3)

$$\frac{\partial \tilde{N}_O}{\partial t} = \frac{1}{v_s}\frac{\partial}{\partial x}\left[D_O\left(\frac{2v_s}{3 - v_s}\right)\frac{\partial \tilde{N}_O}{\partial x}\right] - \frac{K}{v_s}\left[N_H\left(\frac{\tilde{N}_O}{\tilde{N}_{50}}\right)^n - N_{HO}\right] + \frac{\tilde{N}_O \Gamma_2}{v_s C_p} \tag{21}$$

$$\frac{\partial N_{HO}}{\partial t} = \frac{\partial}{\partial x}\left[D_H\left(\frac{2v_s}{3 - v_s}\right)\frac{\partial \tilde{N}_{HO}}{\partial x}\right] + K\left[N_H\left(\frac{\tilde{N}_O}{\tilde{N}_{50}}\right)^n - N_{HO}\right] \tag{22}$$

$$\frac{\partial N_H}{\partial t} = \frac{\partial}{\partial x}\left[D_H\left(\frac{2v_s}{3 - v_s}\right)\frac{\partial \tilde{N}_H}{\partial x}\right] - K\left[N_H\left(\frac{\tilde{N}_O}{\tilde{N}_{50}}\right)^n - N_{HO}\right] - \Gamma_2, \tag{23}$$

where C_p is the polymer density ($= n_H/v_p$) and $v_s = 1 - (n_H/C_p)$. The product of the diffusion coefficient, D_k, and

v_{eff} represents the effective diffusivity of the species "k" in the cell at any given x and t. The term $\tilde{N}_O\Gamma_2/(v_sC_p)$ is a result of the volume change of solution associated with polymerization on $\tilde{N}_O$. The solution volume fraction in the cell decreases with increasing amounts of polymer. This has the effect of decreasing the solution volume "available" to the oxygen molecules and, consequently, increasing $\tilde{N}_O$ (moles O_2 per unit volume of solution). This mechanism of contributing to an increase in $\tilde{N}_O$ can, therefore, be qualitatively thought of as a "concentrating effect." Eq. 4 gives the rate of change of the polymerized monomer concentration.

The red cell membrane is impermeable to hemoglobin and hence, the sum total of moles of the three individual hemoglobin components remains constant for the cell. At any given time t,

$$\int_0^a [N_H(x, t) + N_{HO}(x, t) + n_H(x, t)]\, dx = C_{t,i}, \tag{24}$$

where $C_{t,i} = C_t(t = 0)$. Eq. 24 can be used to check the accuracy of the solutions for Eqs. 4, 22, and 23. Hence, it is convenient to leave the concentrations on the left hand side of these equations in moles per unit cell volume. Molar concentrations per unit solution volume cannot be used in Eq. 24 because the solution volume is not constant.

Scaling the transport and kinetics equations

The transport equations for oxygen and the hemoglobin components are expressed in a nondimensional form by making the concentrations, length, and time dimensionless. Using the superscript "prime" to denote nondimensional quantities, we have $x' = x/a$, $t' = t/ts$, $\tilde{N}'_O = \tilde{N}_O/\tilde{N}_{50}$, $N'_{HO} = N_{HO}/C_{t,i}$, $N'_H = N_H/C_{t,i}$ and $n'_H = n_H/C_{t,i}$. The time scale, ts, is somewhat arbitrarily chosen as $a^2/D_{H,i}$, where $D_{H,i}$ is the hemoglobin diffusivity at time $t = 0$.

Making the appropriate substitutions in Eqs. 4, 21, 22, and 23, we get

$$\frac{\partial \tilde{N}'_O}{\partial t'} = \frac{1}{v_s}\frac{\partial}{\partial x'}\left[D'_O\left(\frac{2v_s}{3 - v_s}\right)\frac{\partial \tilde{N}'_O}{\partial x'}\right] - \frac{K'_1}{v_s}[N'_H(\tilde{N}'_O)^n - N'_{HO}] + \left(\frac{\tilde{N}'_O\Gamma'_2}{v_sC'_p}\right) \tag{25}$$

$$\frac{\partial N'_{HO}}{\partial t'} = \frac{\partial}{\partial x'}\left[D'_H\left(\frac{2v_s}{3 - v_s}\right)\frac{\partial \tilde{N}'_{HO}}{\partial x'}\right] + K'_2[N'_H(\tilde{N}'_O)^n - N'_{HO}] \tag{26}$$

$$\frac{\partial N'_H}{\partial t'} = \frac{\partial}{\partial x'}\left[D'_H\left(\frac{2v_s}{3 - v_s}\right)\frac{\partial \tilde{N}'_H}{\partial x'}\right] - K'_2[N'_H(\tilde{N}'_O)^n - N'_{HO}] - \Gamma'_2 \tag{27}$$

$$\frac{\partial n'_H}{\partial t'} = \Gamma'_2, \tag{28}$$

where $D'_O = D_Ots/a^2$, $D'_H = D_Hts/a^2$, $K'_1 = KtsC_{t,i}/\tilde{N}_{50}$, $K'_2 = Kts$, $\Gamma'_2 = \Gamma_2ts/C_{t,i}$ and $C'_p = C_p/C_{t,i}$.

The equations for the kinetics of deoxy HbS polymerization, in the nondimensional form, are

$$\frac{\partial(n^*_H)'}{\partial t'} = K'_+(\gamma N'_H)\left[(n^*_{H,j^*})' + \frac{(\gamma_{i^*}n^*_{H,i^*})'}{\gamma_{i^*+1}}\right] \tag{29}$$

$$\Gamma'_2 = K'_+[(\gamma N'_H) - (\gamma_{sol}N'_{H,sol})](n^*_H)', \tag{30}$$

where

$$(\gamma_{i^*}n^*_{H,i^*})' = (\gamma_{sol}N'_{H,sol}) \exp[15.6087 \ln(\ln S) - 22.7081] \tag{31}$$

$$(n^*_{H,j^*})' = \phi n'_H \exp[16.6087 \ln(\ln S) - 22.509] \quad S < 3.5099 \tag{32}$$

$$= \phi n'_H \exp[13.2278 \ln S - 35.3375] \quad 3.5099 \le S \le 4.4034 \tag{33}$$

$$= \phi n'_H \exp[2.5419 \ln(\ln S - 1.2902) - 11.5362] \quad S > 4.4034 \tag{34}$$

$$S = \frac{\gamma N'_H}{\gamma_{sol}N'_{H,sol}}. \tag{35}$$

Here, $(n^*_H)' = n^*_H/C_{t,i}$, $N'_{H,sol} = N_{H,sol}/C_{t,i}$, $(n^*_{H,j^*})' = n^*_{H,j^*}/C_{t,i}$, $(\gamma_{i^*}n^*_{H,i^*})' = (\gamma_{i^*}n^*_{H,i^*})/C_{t,i}$ and $K'_+ = K_+tsC_{t,i}$. These transport and polymerization kinetics equations are highly nonlinear and have to be solved numerically.

Boundary conditions

We solve the transport equations for half the cell width due to symmetry. Therefore, we have

$$\left.\frac{\partial \tilde{N}'_O}{\partial x'}\right|_{x'=0} = 0 \tag{36}$$

$$\left.\frac{\partial \tilde{N}'_{HO}}{\partial x'}\right|_{x'=0} = 0 \tag{37}$$

$$\left.\frac{\partial \tilde{N}'_H}{\partial x'}\right|_{x'=0} = 0 \tag{38}$$

at the cell center.

No hemoglobin can pass through the cell membrane and hence, at the cell wall, the boundary conditions on the

free HbS components can be written as

$$\left.\frac{\partial \tilde{N}'_{HO}}{\partial x'}\right|_{x'=1} = 0 \tag{39}$$

$$\left.\frac{\partial \tilde{N}'_{H}}{\partial x'}\right|_{x'=1} = 0. \tag{40}$$

The polymer doesn't undergo diffusion and hence, there is no boundary condition for n'_H.

The remaining boundary condition for free oxygen depends on the situation being modeled. The red cell membrane is assumed to offer no resistance to the transport of O_2 and hence, the most general boundary condition for free oxygen at the surface of the red cell is a matching condition with the external environment. It is much simpler, however, to solve the O_2 transport equation by uncoupling it from the transport dynamics outside the cell.

We concentrate on intra red cell transport in the present study and specify the oxygen partial pressure at the cell surface, $(P_{O_2})_w$. The value of $(P_{O_2})_w$ can be made a function of time to mimic the oxygen environment that a red cell "sees" as it traverses a capillary. This same situation could also be modeled in a different way by imposing a value of oxygen flux on the boundary. In the present model, $(P_{O_2})_w$ is kept constant. The boundary oxygen concentration, $\tilde{N}_{O,w}$ $[= B(x' = 1) \times (P_{O_2})_w]$, however, does not remain constant as polymerization affects the Bunsen solubility of oxygen. This effect is dealt with later.

Initial conditions

In the absence of significant precapillary oxygen losses, the red cell will have a uniform, initial oxygen concentration $\tilde{N}'_{O,i}$, which is in equilibrium with the dimensionless concentration of saturated free hemoglobin, $Y_{s,i}$. Using the Hill equation to represent this initial equilibrium situation, we have

$$\tilde{N}'_{O,i}(x' < 1) = \left(\frac{Y_{s,i}}{1 - Y_{s,i}}\right)^{1/n}. \tag{41}$$

The initial fractional saturation of free hemoglobin is chosen large enough to ensure that the initial solubility, $C_{sol,i}$, is greater than $C_{t,i}$. Thus, at $t = 0$, the cell enters the capillary free of any polymer. The uniform initial concentrations of the Hb components in the red cell are given by

$$N'_{HO,i} = Y_{s,i}, \tag{42}$$

$$N'_{H,i} = 1 - Y_{s,i}, \tag{43}$$

$$n'_{H,i} = 0, \tag{44}$$

and

$$(n^*_{H,i})' = 0. \tag{45}$$

Deoxy HbS solubility

Sunshine et al. (1982) expressed HbS solubility as an empirical function of Y_s by doing a curve fit to their solubility data at 25°C. Their function was in the form of a 15th order polynomial. To facilitate our computations, we modified their function by curve fitting their data to a fifth order polynomial with a correlation coefficient of 0.996. To obtain the functional dependence of C_{sol} on Y_s at 35°C, we used a temperature correction factor $C_{sol,0(35°C)}/C_{sol,0(25°C)} = 0.8814$ (C. T. Noguchi, personal communication). The solubility at 35°C is, therefore,

$$C_{sol(35°C)} = 0.8814\, C_{sol(25°C)}. \tag{46}$$

The final form of the empirical function for nondimensional solubility of sickle hemoglobin, $C'_{sol}(= C_{sol}/C_{t,i})$, at 35°C is

$$C'_{sol} = e'_1 + e'_2 Y_s + e'_3 Y_s^2 + e'_4 Y_s^3 + e'_5 Y_s^4 + e'_6 Y_s^5, \tag{47}$$

where $e'_1 = C_{sol,0} = 2.5156/C_{t,i}$, $e'_2 = 4.5332/C_{t,i}$, $e'_3 = -30.055/C_{t,i}$, $e'_4 = 97.5586/C_{t,i}$, $e'_5 = -129.128/C_{t,i}$, and $e'_6 = 62.1162/C_{t,i}$ with $C_{t,i}$ in millimolar units.

The distribution of HbS among its different components in a sickle red cell unloading oxygen in the capillaries varies with time spent (or location) in the microcirculation. When the cell enters the capillary ($t = 0$), the fractional saturation, Y_s, in our model is high enough for all the hemoglobin in the cell to be in a soluble form. This condition persists as long as C'_{sol} remains greater than one, and the sickle cell unloads oxygen like a normal cell. A mass balance of the species in the cell gives

$$C'_t(=1) = N'_{HO} + N'_H, \tag{48}$$

where $C'_t = C_t/C_{t,i}$, $N'_{HO} = Y_s$, and $N'_H = 1 - Y_s$. Y_s decreases as the cell unloads oxygen in the capillaries and reaches a critical saturation, $Y_{s,cr}$, at time $t = t_{cr}$. At this instant, the hemoglobin solution in the cell reaches the critical saturation $C'_{sol}(Y_{s,cr}) = 1$.

The HbS solution becomes supersaturated for $t > t_{cr}$ and the deoxy HbS monomer starts aggregating. The mass balance of the species now gives

$$C'_t = N'_{HO} + N'_H + n'_H. \tag{49}$$

Although the total hemoglobin concentration averaged over the cell remains constant (Eq. 24), $C'_t(x, t)$ is not necessarily equal to 1 throughout the cell, due to the diffusive redistribution of the hemoglobin components. To

determine the degree of supersaturation, S, we express N'_H as the sum of two subcomponents; one that is soluble in the HbS solution at equilibrium, $N'_{H,sol}$, and the other that is in excess of the soluble part (the supersaturated part), $N'_{H,sup} = N'_H - N'_{H,sol}$. We should mention here that there is no real physical separation of these two components and they cannot be distinguished from one another in the solution. However, this step is essential for determining $N'_{H,sol}$ at any instant t. In the theoretical model for the laser photolysis experiment (Ferrone et al., 1985*b*), this $N'_{H,sol}$ corresponds to the deoxy HbS solubility, $C'_{sol,0}$, which is a known constant. In the present model, the solubility C'_{sol} represents soluble moles of oxy and deoxy HbS. Hence the need for splitting the HbS components in the solution ($N'_{H,O} + N'_H$) into the soluble part ($N'_{HO} + N'_{H,sol}$) and the supersaturated part ($N'_{H,sup}$).

We assign hypothetical volume fractions to the soluble and the supersaturated HbS "components" in the solution, v_{sol} and v_{sup}, respectively, where $v_{sol} + v_{sup} = v_s$. Because the cell comprises of solution and polymer, we have

$$1 = v_{sol} + v_{sup} + v_p. \tag{50}$$

We use the specific volume of the unaggregated deoxy HbS monomer (= 0.79 cc/g), given by Minton (1983), to get the density of the unaggregated monomer, C_H (= 1.2658 g/cc monomer). The polymer density, C_p, is taken equal to 0.69 g/cc polymer (Sunshine et al., 1979). We rewrite Eq. 49 as

$$C'_t = (N'_{HO} + N'_{H,sol}) + N'_{H,sup} + n'_H \tag{51}$$

$$= v_{sol} C'_{sol} + v_{sup} C'_H + v_p C'_p, \tag{52}$$

where $C'_H = C_H/C_{t,i}$ with $C_{t,i}$ in g/cc.

The solubility and fractional saturation data of Sunshine et al. (1982) were obtained for HbS solution samples in which the polymer was in equilibrium with the rest of the solution. This indicates that the deoxy HbS in their solution samples corresponds to $N_{H,sol}$ in our model and, therefore, the fractional saturation, Y_s, used in the empirical relationship (Eq. 47) is

$$Y_s = \frac{N'_{HO}}{N'_{HO} + N'_{H,sol}} = \frac{N'_{HO}}{v_{sol} C'_{sol}}. \tag{53}$$

Eqs. 47 and 50–53 can be solved simultaneously (see Appendix 4) to obtain a polynomial of the form

$$\sum_{i=0}^{6} a_{i+1} Y_s^i = 0, \tag{54a}$$

where

$$a_1 = Q(C'_H - e'_1) \tag{54b}$$

$$a_i = e'_{i-1} - Qe'_i \quad \{i = 2 - 6\} \tag{54c}$$

$$a_7 = e'_6 \tag{54d}$$

$$Q = \frac{N'_{HO} C'_p}{C'_p(C'_t - n'_H) - C'_H(C'_p - n'_H)}. \tag{54e}$$

Y_s corresponds to the real, nonnegative root of the polynomial. From Eq. 53, the soluble deoxy HbS component is

$$N'_{H,sol} = N'_{HO}\left(\frac{1 - Y_s}{Y_s}\right). \tag{55}$$

$N_{H,sol}$ approaches the value of $C'_{sol,0}$ as the cell continues to unload oxygen. Although the amounts of polymer present in the cell are negligible for $t_{cr} < t < t_{cr} + t_d$, we still use the above technique for determining $N'_{H,sol}$ for all $t > t_{cr}$ to ensure continuity of $n'_H = n'_H(t')$ and $\Gamma'_2 = \partial n'_H/\partial t'$.

Parameter values

There are three important parameters that influence the theoretical results obtained from the present model for a given temperature and plasma pH; the total hemoglobin concentration in the cell, $C_{t,i}$, the boundary PO_2 and the 2,3-DPG/Hb molar ratio (*M.R.*). $C_{t,i}$ and *M.R.* affect the values of kinetic constants and diffusion coefficients used in the model. $C_{t,i}$ also influences the actual physical processes involved in the unloading phenomenon through the number of HbS moles that are "allowed" to polymerize. The boundary PO_2 doesn't have any effect on the constants/coefficients used in the model. Its influence on the oxygen delivery process is manifested through its effect on oxygen concentration gradients. In this section, we look at the effect of $C_{t,i}$ and *M.R.* on the kinetic constants and diffusion coefficients.

We take a typical value of 0.34 g/cc for the hemoglobin density within the red cell. For a 64 kD molecular weight of Hb, this density corresponds to a hemoglobin concentration of

$$C_{t,i} = 5.3125 \text{ mM}. \tag{56}$$

The plasma pH is taken as 7.4.

The diffusion coefficient of oxygen (D_O) is obtained from the compilation of data by Kreuzer (1970); hemoglobin diffusivity (D_H) is taken from the measurements of Spaan et al. (1980). The functional dependence of these diffusivities on the solution hemoglobin concentration, [Hb] (= $\tilde{N}_{HO} + \tilde{N}_H$) is given in Appendix 5. Polymerization alters the hemoglobin concentration in the solution and this results in a spatial and temporal variation of the diffusion coefficients. The initial values of the two diffusivities at 35°C, corresponding to a hemoglobin density of

0.34 g/cc, are (see Appendix 5):

$$D_{H,i} = 1.454 \times 10^{-7}\ \text{cm}^2/\text{s} \quad (57)$$

$$D_{O,i} = 8.797 \times 10^{-6}\ \text{cm}^2/\text{s}. \quad (58)$$

We now consider kinetic parameters which are quite sensitive to the 2,3-DPG/Hb molar ratio. For normal cells, we choose a characteristic molar ratio of 1 (MacDonald, 1977). Because 2,3-DPG concentrations are elevated in sickle red cells, the molar ratio being as high as 2 in some cases (Charache et al., 1970; Jensen et al., 1973), we choose a value of $M.R. = 1.5$ to represent the intraerythrocyte DPG concentration.

The kinetic parameters are influenced by the molar ratios. If these molar ratios were to be altered by the presence of polymer, then the kinetic parameters would vary during the course of oxygen unloading/HbS polymerization. We assume, at this stage, due to lack of information on the affinity of the polymer for 2,3-DPG, that the polymer has the same affinity for the diphosphoglycerate as the solution phase T-state molecules and that deoxy monomer aggregation doesn't inhibit the binding of 2,3-DPG. Then the molar ratio of 2,3-DPG/Hb does not change during polymerization. In any case, our model incorporates only the first 15% of the curve for localized growth of polymer and it is unlikely that such small amounts of polymer would alter the molar ratio significantly.

We get P_{50} from the equations by Samaja et al. (1981) relating human blood P_{50} to $M.R.$, P_{CO_2}, and pH_e at a temperature of 37°C. On using their equations for $pH_e = 7.4$, $P_{CO_2} = 40$ Torr, and applying the temperature correction factor from Kelman and Nunn (1966), we get, at 35°C (see Appendix 6),

$$P_{50} = 26.34\ \text{Torr} \quad M.R. = 1 \quad (59)$$

$$= 29.84\ \text{Torr} \quad M.R. = 1.5. \quad (60)$$

The Bunsen solubility coefficient, B, is needed to convert P_{50} to N_{50} and P_{O_2} to N_O. Spaan et al. (1980) have given a formula that determines B from the value of B_{H_2O}, the Bunsen solubility for water, taking into account the increase in solubility due to hemoglobin and the corresponding decrease due to dissolved salts. If we ignore the correction for salt concentrations, which is very small, their formula reduces to

$$B = B_{H_2O}(1 + 1.997 \times 10^{-2}\,[Hb]), \quad (61)$$

where $[Hb]$ is in millimolars. The value of B_{H_2O} at 35°C, obtained from the standard solubility tables by Linke (1965), is 1.459×10^{-3} mM/Torr. Polymerization alters $[Hb]$ and, consequently, the solubility of oxygen.

The effect of molar ratio on the Hill's parameter, n, at constant P_{CO_2} and pH_e is given by Winslow et al. (1983) for a temperature of 37°C. We assume that these values of n remain unchanged at 35 °C and get

$$n = 2.63 \quad M.R. = 1 \quad (62)$$

$$= 2.67 \quad M.R. = 1.5. \quad (63)$$

The dissociation rate constant, K, is highly sensitive to temperature, pH, and the molar ratio. Due to lack of extensive published data on the variation of K with these three parameters, the values of K at the desired physiological conditions are obtained by making certain assumptions and interpolating the data (see Appendix 6) from Salhany et al. (1970) and Bauer et al. (1973).

The internal pH of the red cell solution is determined using the nomogram from Samaja and Winslow (1979) for ΔpH across the red cell membrane. For $pH_e = 7.4$, we get

$$pH_i = 7.22 \quad M.R. = 1 \quad (64)$$

$$= 7.16 \quad M.R. = 1.5. \quad (65)$$

We estimate the value of K, at 35°C and the respective hemoglobin solution pH's, to be (see Appendix 6)

$$K = 167\ s^{-1} \quad M.R. = 1 \quad (66)$$

$$= 179\ s^{-1} \quad M.R. = 1.5. \quad (67)$$

An important non kinetic parameter in our model, that is also sensitive to molar ratios, is the deoxy HbS solubility, $C_{sol,0}$. However, this sensitivity is restricted to molar ratios <1 (Poillon et al., 1986), and thus we do not consider it further here.

We choose two values of hemoglobin densities, 0.324 g/cc ($C^A_{t,i} = 5.0625$ mM) and 0.362 g/cc ($C^B_{t,i} = 5.6563$ mM), to study the effect of $C_{t,i}$ on the unloading of O_2 from sickle cells. These values correspond to the MCHC's used by Seakins et al. (1973) in their experiments designed to determine the effect of HbS concentration on the oxygen affinity of blood in sickle cell anemia. We use our theoretical model to do a parallel comparison and also determine the individual effects of HbS concentration and elevated molar ratios on the oxygen unloading curve. We use the same values of external pH ($pH_e = 7.13$) and 2,3-DPG/Hb molar ratios (21.8 μmol/g $Hb = 1.4$ and 17.7 μmol/g $Hb = 1.13$) as Seakins et al. (1973). The temperature is constant at 35°C and $P_{CO_2} = 40$ Torr.

We get the initial values of diffusivities, corresponding to these hemoglobin densities, from the functions given in Appendix 5

$$D^A_{O,i} = 9.393 \times 10^{-6}\ \text{cm}^2/\text{s} \quad (68)$$

$$D^B_{O,i} = 8.029 \times 10^{-6}\ \text{cm}^2/\text{s} \quad (69)$$

$$D^{A}_{H,i} = 1.748 \times 10^{-7}\ \text{cm}^2/\text{s} \quad (70)$$

$$D^{B}_{H,i} = 1.021 \times 10^{-7}\ \text{cm}^2/\text{s}. \quad (71)$$

The kinetic parameters, P_{50}, n, and K, for the two molar ratios are obtained using the procedure outlined in Appendix 6. The final values of these parameters, at $P_{CO_2} = 40$ Torr, $pH_e = 7.13$, and $T = 35°C$, are

$$P_{50} = 34.4\ \text{Torr} \quad M.R. = 1.13 \quad (72)$$

$$P_{50} = 36.72\ \text{Torr} \quad M.R. = 1.4 \quad (73)$$

$$K = 190.6\ \text{s}^{-1} \quad M.R. = 1.13 \quad (74)$$

$$K = 198.4\ \text{s}^{-1} \quad M.R. = 1.4. \quad (75)$$

The Hill coefficient, n, from Winslow et al. (1983), is 2.64. The Bunsen solubility coefficient is determined using Eq. 61.

Finally, we choose three values of hemoglobin density, 0.35 g/cc ($C^1_{t,i} = 5.4688$ mM), 0.34 g/cc ($C^2_{t,i} = 5.3125$ mM), and 0.33 g/cc ($C^3_{t,i} = 5.1563$ mM), to study the effect of hemoglobin concentration on intracellular polymerization in sickle erythrocytes. The initial values of the diffusion coefficients at hemoglobin densities of 0.33 and 0.35 g/cc, from Appendix 5, are:

$$D^1_{O,i} = 8.440 \times 10^{-6}\ \text{cm}^2/\text{s} \quad (76)$$

$$D^3_{O,i} = 9.166 \times 10^{-6}\ \text{cm}^2/\text{s} \quad (77)$$

$$D^1_{H,i} = 1.262 \times 10^{-7}\ \text{cm}^2/\text{s} \quad (78)$$

$$D^3_{H,i} = 1.639 \times 10^{-7}\ \text{cm}^2/\text{s}. \quad (79)$$

The values of $D^2_{H,i}$ and $D^2_{O,i}$ have been listed earlier (Eqs. 57 and 58, respectively).

Numerical solution

A simulation of oxygen unloading from sickle cells in the presence of HbS polymerization requires solving the transport equations (25–28), polymerization kinetic equations (29–35 and A2.1–A2.3) and the deoxy HbS solubility equations (54*a*–55) simultaneously. Attempting an analytical solution of these highly nonlinear, coupled, partial differential equations would be extremely difficult. We, therefore, need a numerical technique for solving the governing partial differential equations. The problem associated with numerical integration of the coupled transport equations is that of stringent stability requirements for the numerical algorithm. This, however, can be tackled by "trial and error" experimentation with the choice of grid intervals.

We develop a numerical algorithm, using an explicit finite difference scheme with nondimensional grid spacings $\Delta x'$ and $\Delta t'$ ($\Delta x'$, $\Delta t'$ constant). A well-established stability criterion for numerical integration of a linear diffusion equation ($\partial N/\partial t = D\partial^2 N/\partial x^2$), using an explicit finite difference algorithm, is

$$\frac{\Delta t D}{\Delta x^2} \le \frac{1}{2}, \quad (80)$$

where D is the diffusivity. The stability criterion for the nonlinear transport equations is not known a priori. However, we can expect it to be at least as stringent as the above criterion.

We used 15 grid points (nodes) in the cell half width ($0 \le x' \le 1$) with the 1st and 15th node coinciding with the cell center and boundary, respectively. Then for a uniform grid

$$\Delta x' = \frac{1}{14}. \quad (81)$$

For the time step, we used

$$\Delta t' = 3 \times 10^{-5}. \quad (82)$$

The stability criterion (Eq. 80 written in a nondimensional form) is satisfied with this $\Delta x'$ and $\Delta t'$ for all initial values of effective diffusivity for both species, $D'_{H,i}$ and $D'_{O,i}$ ($\upsilon_{eff} = 1$ at $t' = 0$). These choices also proved to give a stable algorithm for all cases that we considered in spite of the variation in effective diffusivities of oxygen and hemoglobin (due to the effect of polymerization on the diffusion coefficients and υ_{eff}).

The input parameters in our numerical algorithm are $C_{t,i}$, $Y_{s,i}$, $M.R.$, and $(P_{O_2})_w$. The partial differential equations are expressed explicitly in an algebraic form using finite differencing. The first and second order spatial derivatives in the transport equations are expressed in the centered difference form for the internal nodes ($0 < x' < 1$). They are handled somewhat differently at the boundary nodes (see Appendix 7). The first order time derivatives of concentration are approximated using the forward differencing scheme and the concentrations of O_2 and the HbS components at any node in the cell at a time $t' + \Delta t'$ are determined from their corresponding values at time t'.

HbS solubility is determined at each step from Eq. 47, using $Y_s = N'_{HO}$, to check for the initiation of polymerization. We bypass the polymerization kinetic equations for $t \le t_{cr}$ to avoid dealing with singularities arising from the "ln(ln S)" term in Eqs. 31 and 32 (because $S = 1$) and impose values of $n'_H = 0$, $\Gamma'_2 = 0$ on Eqs. 25–28. Once $C'_{sol} < 1$ (i.e., $t > t_{cr}$), we get $(n^*_H)'$ and n'_H at time $t' + \Delta t'$ using $S(t')$ obtained from Eqs. 54*a*–55 and A2.1–2.3. Using the values of n'_H and υ_p ($= n'_H/C'_p$), we obtain υ_{eff} and $[Hb]$ and, subsequently, new values of the effective diffusivities at time $t' + \Delta t'$. The boundary oxygen concentration is modified to account for the change in

$B(x' = 1)$, effected by the change in $[Hb]$ at the cell wall. Thus, we get the spatial profiles of $\tilde{N}'_O$, N'_H, N'_{HO}, and n'_H as a function of time for a given set of input parameters and initial values (Eqs. 41–45). The spatial variation of P_{O_2} across the cell is obtained from the spatial profile of $\tilde{N}'_O$ after taking into account the alteration of solubility by the polymer. Concentration profiles are averaged over the cell half width to obtain the variation of averaged concentrations of the various species in the cell with time. Because most of the oxygen in the cell is bound to Hb, the variation of $N'_{HO,avg}$ with time is representative of the oxygen unloading process. $n'_{H,avg}(t')$ indicates the extent of HbS polymerization in the cell at any instant t'.

The numerical algorithm is also used to simulate oxygen delivery from normal red cells by replacing the solubility expression (Eq. 47) with

$$C'_{sol} = \text{constant } (>1). \tag{83}$$

Because the criterion for initiation of polymerization is never satisfied in the algorithm for this case, it continues to simulate oxygen unloading from normal cells analogous to the earlier part of the oxygen delivery process from sickle cells ($t < t_{cr}$).

Finally, we extend our two phase model to the equilibrium situation to reproduce the equilibrium oxygen dissociation curve for sickle hemoglobin at fixed values of $M.R.$ and $C_{t,i}$. We assume equilibrium between (a) deoxy HbS in the polymer and in the solution (with $S = 1$ everywhere in the cell), and, (b) oxygen and oxy HbS in the solution. The mole fractions of polymer and solution in the cell, at any given P_{O_2} and $C_{t,i}$, are obtained from mass balance (Ross et al., 1977). Because there is no oxygen incorporated into the polymer in our model, the total fractional oxygen saturation, Y_t, at any given P_{O_2} is the product of Y_s and the mole fraction of the solution, x_s. The details of this equilibrium analysis are given in Appendix 8.

The numerical algorithm was used, in both the sickle and normal cell modes, to analyze several different cases. We used fixed values of $Y_{s,i} = 0.95$ and $T = 35°C$ in all our analyses. The variation of spatial profiles and the spatially averaged values of oxygen and the hemoglobin components with time were determined for sickle and normal cells with a hemoglobin density of 0.34 g/cc. This was done at molar ratios of 1 and 1.5 and boundary P_{O_2}'s of 0, 5, 10, 15, and 20 Torr with $pH_e = 7.4$. The equilibrium model was used to determine the maximum extent of desaturation possible in these cases from the equilibrium values of total oxygen fractional saturation at the respective P_{O_2}'s. The effect of hemoglobin concentration on the extent of polymerization in sickle cells was also studied by doing computations for cells with $C_{t,i} = 0.33$, 0.34, and 0.35 g/cc. The molar ratio was taken as 1.13, plasma pH, 7.13 and boundary P_{O_2}, 20 Torr. Finally, to establish the individual effects of hemoglobin concentration and molar ratio on the rate of O_2 unloading from sickle cells, we ran the numerical code for cells with hemoglobin densities of 0.324 and 0.362 g/cc and molar ratios, 1.13 and 1.4, keeping $(P_{O_2})_w$ constant at 20 Torr and pH_e at 7.13. We also used the equilibrium model to study the relative effects of these two parameters ($C_{t,i}$ and $M.R.$) on the oxygen affinity of sickle hemoglobin (based on the equilibrium oxygen dissociation curve).

Computations for the sickle cell cases were done till the point where the maximum polymer concentration in the cell reached a value that was 15% of the equilibrium polymer concentration at zero fractional saturation. The computations were then repeated for the same number of iterations in the normal cell mode. To check for the accuracy of our solutions, we made several runs for some of the above cases using smaller time steps ($\Delta t' = 1 \times 10^{-5}$ and 2×10^{-5}) and compared the results with those obtained for $\Delta t' = 3 \times 10^{-5}$. The maximum discrepancy between corresponding values of concentration for any species, obtained using smaller time steps, was within 0.5% of the original results.

Results and discussion

The characteristic spatial profiles of the concentration variables were plotted for sickle and normal cells. We also plotted the oxygen unloading and polymerization curves for sickle cells and tried to establish the individual effects of 2,3-DPG concentration, $(P_{O_2})_w$ and $C_{t,i}$ on these processes.

Fig. 3 shows the spatial variation of C'_t in the sickle red cell, during the unloading and polymerization process. The shape of the curve indicates a net diffusive redistribution of the HbS components across the cell width. The O_2 gradients in the vicinity of the cell wall are quite steep, resulting in the fastest rate of decrease of Y_s and, subsequently, C_{sol}. The criterion for polymerization is first satisfied at the outermost node in the cell and results in the buildup of polymer in this region. HbS accumulation at the wall is compensated by a corresponding decrease in concentration towards the center of the cell. This variation is absent in normal cells.

The three important mechanisms of deoxygenation, diffusion and polymerization (see Fig. 1) influence, directly or indirectly, the relative amounts of oxygen and the three HbS components present in the cell at any given instant. The polymer concentration is directly influenced by polymerization kinetics; the other two mechanisms affect it indirectly through their influence on the number of deoxy HbS moles "available" for polymerization at any given point in the cell. Polymerization affects N'_{HO} and $\tilde{N}'_O$ indirectly through its influence on the other two

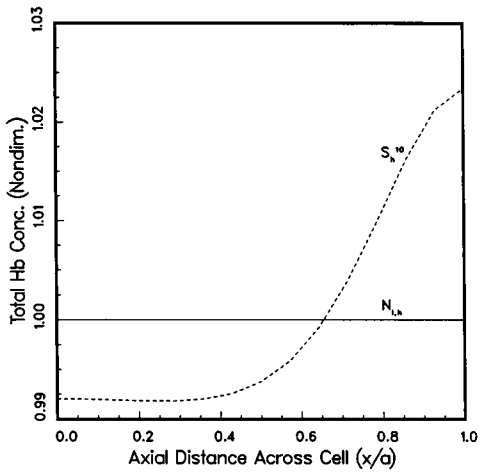

FIGURE 3 Spatial profile of the nondimensional total hemoglobin concentration, C'_t, in the cell half width, during the O_2 unloading process, at $t = 0.153$ s in normal cells ($N_{1,h}$:molar ratios of 1 and 1.5) and sickle cells (S_h^{10}:molar ratio = 1.5, $(P_{O_2})_w = 10$ Torr) with a hemoglobin density of 0.34 g/cc. The plasma pH is 7.4. Also, $a = 1$ μm.

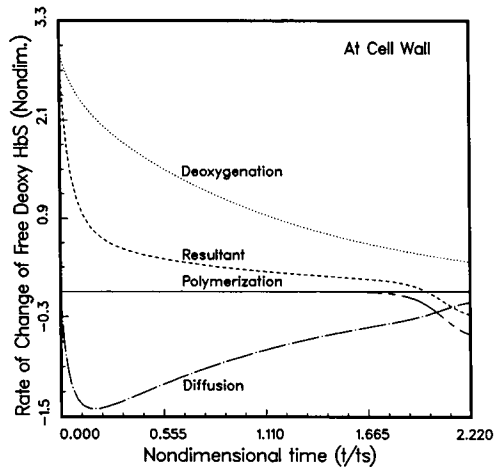

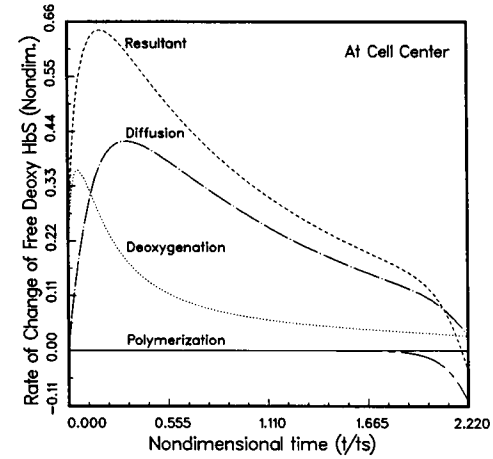

FIGURE 4 Rate of change of nondimensional, free deoxy HbS concentration, N'_H with t' $(=t/ts)$, due to diffusion, deoxygenation, and polymerization, as a function of t' at (a) the cell wall, and, (b) the cell center, for sickle cells with a hemoglobin density of 0.34 g/cc, molar ratio 1.5 and 10 Torr boundary P_{O_2}. $pH_e = 7.4$ and $ts = 0.0688$ s.

mechanisms. Deoxyhemoglobin concentrations, however, are directly affected by all three processes. A study of the rate of change of N'_H, due to these three separate mechanisms, at both extremes of the domain (i.e., the cell center and cell wall) gives insight into the relative magnitudes of the effect of these three mechanisms at different stages of the oxygen delivery process.

Figs. 4, a and b show the separate influences of deoxygenation, diffusion, and polymerization on $\partial N'_H/\partial t'$ (obtained from Eq. 27) at the cell wall and cell midpoint, respectively. At $t' = 0$, the cell enters the microcirculation with a 95% oxygen fractional saturation and encounters a very low oxygen environment. This triggers off a rapid HbO_2 dissociation reaction in the vicinity of the cell wall and disturbs the spatial homogeneity of the HbS components in the cell. The disturbance propagates to the cell center, subsequently resulting in diffusive fluxes throughout the cell. The deoxygenation reaction contributes toward an increase in N'_H at all points in the cell (see Fig. 1). Diffusion slows down the rapid increase in deoxy HbS concentration near the cell boundary, where the dissociation rate is maximum, by passive transport of deoxyhemoglobin S toward the cell interior. This diffusive transport assists the accumulation of deoxy HbS monomers in the regions of slow deoxygenation near the cell center. Thus, deoxygenation and diffusion affect the resultant $\partial N'_H/\partial t'$ in an opposite sense at the cell wall (Fig. 4 a) and in a complementary sense at the cell center (Fig. 4 b). The large concentration gradients, resulting from the initial disturbance, start leveling off gradually and lead to a decrease in diffusion and deoxygenation rates. This slows down the rate of increase of N'_H everywhere in the cell.

Polymerization first begins at the cell wall at $t' = t'_{cr}$ and slowly propagates to the cell interior. The autocatalytic growth of polymer, at the end of the delay period, rapidly removes deoxy HbS monomers from the supersaturated HbS solution. The polymerization reaction now acts in conjunction with the diffusion mechanism at the cell boundary to counter the increase in N'_H due to oxyhemoglobin dissociation. At the cell center, polymer formation opposes both deoxygenation and diffusion. The rate of polymer growth soon becomes large enough to cause N'_H to decrease, first at the cell wall, and then, subsequently, at other points in the interior of the domain. This transition can be seen in Figs. 4, a and b at the point

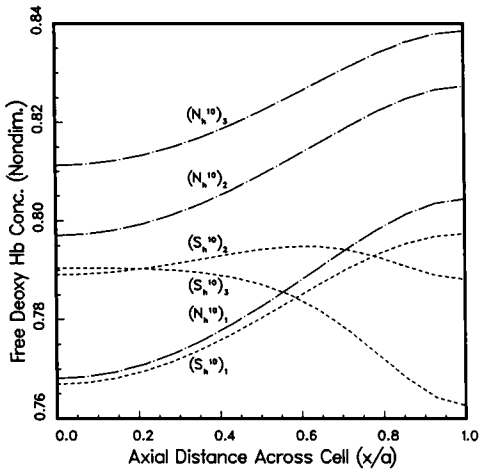

FIGURE 5 Spatial profile of nondimensional, free deoxyhemoglobin concentration, N'_H, in the cell half width at three different stages during the oxygen unloading process (1:t = 0.132 s; 2:t = 0.145 s; 3:t = 0.153 s) in normal (N_h^{10}:$M.R.$ = 15, $(P_{O_2})_w$ = 10 Torr) and sickle (S_h^{10}:$M.R.$ = 1.5, $[P_{O_2}]_w$ = 10 Torr) cells with a hemoglobin density of 0.34 g/cc. Plasma pH is 7.4 and a = 1 μm.

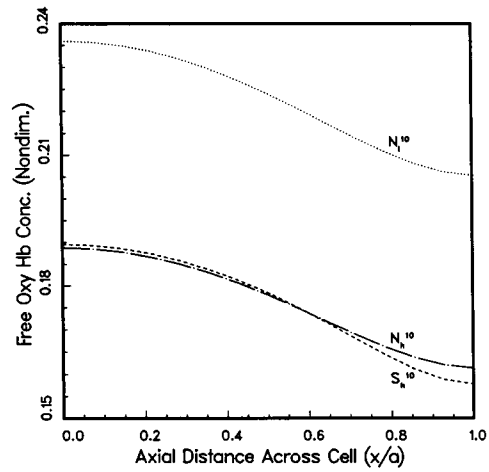

FIGURE 6 Spatial profile of nondimensional, free oxyhemoglobin concentration, N'_{HO}, in the cell half width, during the O_2 unloading process, at t = 0.153 s for normal (N_1^{10}, N_h^{10}:molar ratios of 1 and 1.5, respectively; $[P_{O_2}]_w$ = 10 Torr) and sickle (S_h^{10}:molar ratio = 1.5, $[P_{O_2}]_w$ = 10 Torr) cells with a hemoglobin density of 0.34 g/cc. pH_e = 7.4 and a = 1 μm.

where the "resultant" curve intersects the X-axis ($\partial N'_H/\partial t' = 0$).

The variation in the spatial concentration profiles of deoxy HbS and deoxy HbA are shown in Fig. 5. In normal cells, the deoxyhemoglobin concentration increases monotonically throughout the cell width with $N'_H(x' = 1) > N'_H(x' = 0)$ due to the higher deoxygenation rates at the cell boundary. In sickle cells, the deoxyhemoglobin concentration increases initially analogous to the case for normal cells. The spatial profile of deoxy HbS at t = 0.132 s in Fig. 5 represents a typically "growing" profile. At t = 0.153 s, polymerization rates in the cell are large enough to cause N'_H to decrease everywhere in the domain. The fact that the decrease in deoxy HbS concentration is faster near the cell membrane as compared with the rest of the cell indicates the higher rates of polymer growth in that region. The spatial profile at t = 0.145 s shows $N'_H(x')$ in the transition state. The difference between corresponding deoxyhemoglobin concentrations in sickle and normal cells at any spatial position in Fig. 5 represents the amount of deoxy HbS monomer incorporated into the polymer at that location in the cell.

Lowered O_2 affinity in normal cells with higher 2,3-DPG concentrations results in lowered oxyhemoglobin concentrations. This can be seen from the spatial profiles of N'_{HO} for normal cells with molar ratios of 1 and 1.5 in Fig. 6. The rate of deoxygenation is always higher in the vicinity of the cell wall and, hence, $N'_{HO}(x' = 1) < N'_{HO}(x' = 0)$.

The spatial variation of N'_{HO} in sickle cells, relative to that in normal cells with the same 2,3-DPG concentration, is difficult to visualize intuitively. The rate of change of N'_{HO} in either cell is directly influenced by the deoxygenation and diffusion of oxyhemoglobin. The former tends to decrease oxyhemoglobin concentrations throughout the cell width. The latter, however, decreases N'_{HO} only in the vicinity of the cell center. Diffusion tends to replenish the oxyhemoglobin dissociated at the cell boundary. Polymerization affects the rate of change of oxyhemoglobin and, consequently, the oxygen unloading process indirectly through its interference with these two mechanisms. The nature and the extent of interference of polymerization with deoxygenation and diffusion depends on the relative magnitudes of the three mechanisms at any instant.

An important parameter that influences the effect of intracellular polymerization on the other two mechanisms is the boundary P_{O_2}. We compared the oxygen unloading curves for sickle and normal cells having the same $C_{t,i}$ and 2,3-DPG concentration for different values of $(P_{O_2})_w$. On plotting the variation of $N'_{HO,avg}$(sickle)/$N'_{HO,avg}$ (normal) with time (see Fig. 7), we found a reversal in the trend of variation for the 0 and 5 Torr case. Normal cells seem to unload oxygen faster than sickle cells for $(P_{O_2})_w$ = 0 Torr (indicated by a ratio >1 which increases monotonically). However, with a boundary P_{O_2} of 5, 10, and 15 Torr, sickle cells seemed to have a lower affinity for oxygen than their normal counterparts. To explain this anomaly in the characteristics of the oxygen unloading curves for sickle cells, we need to analyze in detail, the effect of polymerization on the HbO_2 dissociation reaction and the diffusion of

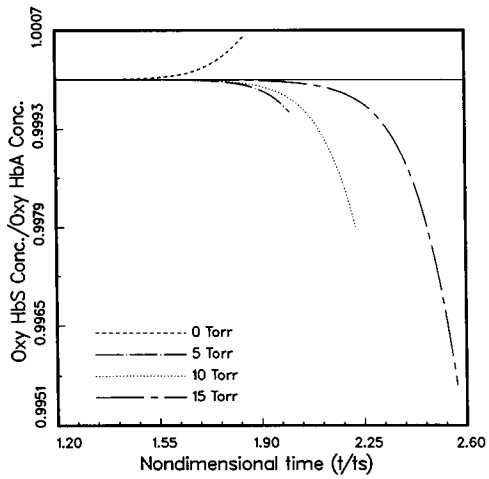

FIGURE 7 The effect of polymer on the oxygen unloading process in sickle cells, represented by the variation with t' ($=t/ts$) of the ratio of nondimensional, spatially averaged, free oxyhemoglobin concentration, $N'_{HO,avg}$, in sickle cells over that in normal cells for $(P_{O_2})_w = 0$, 5, 10, and 15 Torr. The hemoglobin density is 0.34g/cc, $M.R.$ = 1.5, pH_e = 7.4, and ts = 0.0688 s.

oxyhemoglobin S under different P_{O_2} boundary conditions.

HbS polymerization decreases the solution hemoglobin concentration in the cell; this results in an increase in the diffusivity of oxyhemoglobin (and oxygen). The polymer domains in the cell also pose as impenetrable barriers to the motion of HbO_2 molecules. The decrease in effective diffusivity of oxyhemoglobin S due to the latter effect, however, isn't as large as the increase due to the former. Therefore, the effective diffusivity of oxy HbS increases in the presence of polymer. The polymer also lowers the spatial concentration gradients of oxyhemoglobin in the solution ($\partial \tilde{N}'_{HO}/\partial x'$ and $\partial^2 \tilde{N}'_{HO}/\partial x'^2$). This decrease in the concentration gradients is only partially compensated for by the increase in effective diffusivity (at least during the initial part of the polymerization process for the cases considered here). HbS gelation, therefore, results in lower diffusive fluxes of oxyhemoglobin in the cell. This tends to increase N'_{HO} at the cell center and decrease it at the cell edge relative to the oxy HbA concentration in a normal cell. The boundary P_{O_2} doesn't in any way change the nature of the interference of polymerization with the diffusion process. The key to the explanation for the reversal in trend, therefore, lies in the effect of HbS gelation on the deoxygenation reaction kinetics under different conditions of oxygen unloading.

The growth of polymer influences the concentrations of each component involved in the deoxygenation reaction individually. The net effect of polymerization on the deoxygenation reaction rate is dependent on the relative magnitudes of its individual effects on $\tilde{N}'_O$, N'_{HO}, and N'_H. Because N'_H is the only concentration which is directly affected by polymerization kinetics, the primary influence of Γ'_2 on the deoxygenation kinetics is through its effect on the deoxy HbS concentration. The deoxygenation reaction rate in normal cells decreases as deoxy HbA concentration increases monotonically. As discussed earlier, N'_H in sickle cells increases only up to a certain point and then starts decreasing due to the explosive growth of polymerized aggregates (the "sink" effect). This tends to increase the rate of HbO_2 dissociation. We examine this effect more closely in the vicinity of the cell wall, where the rate of polymerization is maximum.

The net deoxygenation term in Eq. 26 can be rewritten for the node at the cell boundary as

$$\text{Deoxygenation term} = K'_2[N'_H(0.0) - N'_{HO}] \quad (P_{O_2})_w = 0 \text{ Torr} \quad (84)$$

$$= K'_2[N'_H(0.0085) - N'_{HO}] \quad (P_{O_2})_w = 5 \text{ Torr} \quad (85)$$

$$= K'_2[N'_H(0.054) - N'_{HO}] \quad (P_{O_2})_w = 10 \text{ Torr.} \quad (86)$$

The deoxygenation term in Eq. 84 is unaffected by N'_H or any variation in the trend of $\partial N'_H/\partial t'$. The polymerization process, therefore, exerts only a very weak influence on deoxygenation kinetics in the region near the cell wall, the primary effect being that of slower diffusion of oxy HbS toward the wall. The cell tries to offset, to some extent, this interference with the compensatory mechanism of diffusion by effectively slowing down HbO_2 dissociation near the cell wall. Polymerization, therefore, results in slower deoxygenation in this region. This type of indirect interference by the polymer is characteristic of situations where the effect of Γ'_2 on $\partial N'_H/\partial t'$ goes virtually "unnoticed" by the deoxygenation mechanism. The slower diffusion and deoxygenation processes contribute individually to $\partial N'_{HO}/\partial t'$ in an opposite sense. The effect of the polymer on diffusion is greater; hence N'_{HO} at the cell wall is lower in sickle cells as compared to normal cells.

The situation at the cell center is more complex than at the wall because all three concentrations are involved in the deoxygenation process for any boundary condition. The polymer interferes with the diffusion of oxy HbS and oxygen away from, and the transport of deoxy HbS toward, the reaction site. The end result of the individual effects of polymerization on N'_{HO}, N'_H, and $\tilde{N}'_O$, for $(P_{O_2})_w = 0$ Torr, is a slower rate of deoxygenation in the sickle cell at the center. The polymer, therefore, interferes with mechanisms of diffusion and deoxygenation in the same sense in this region. As a result, they both contribute toward an increase in N'_{HO} at $x' = 0$ with the effect of slower diffusion more prominent than that of slower

deoxygenation. Owing to the fact that at the cell wall, the effect of slower diffusion on N'_{HO} is partially offset by the slower rate of deoxygenation, a major portion of the cell has a higher N'_{HO}. This results in a higher spatially averaged concentration of oxyhemoglobin S in the sickle cell. Hence, polymerization tends to slow down the unloading of oxygen from a sickle cell when the boundary P_{O_2} is 0 Torr.

The HbO_2 dissociation reaction at the cell boundary is influenced by the decreasing deoxy HbS concentration when the boundary P_{O_2} is 10 Torr (see Eq. 86). The forward dissociation reaction gets accelerated due to the incorporation of deoxy monomers into the polymerized aggregates. The faster deoxygenation reaction, coupled with a slower diffusion (or compensatory) process, rapidly decreases $N'_{HO}(x' = 1)$ and produces a much lower oxyhemoglobin concentration in the vicinity of the cell membrane as compared with the earlier case. The polymer exerts a similar influence on deoxygenation and diffusion at the cell center in the 10 Torr case as in the earlier situation with 0 Torr boundary P_{O_2}, at least during the initial stages of polymerization. Thus, as seen in Fig. 6, $N'_{HO}(x' = 0)$ is higher in sickle cells. The region near the cell boundary, however, experiences a greater effect of polymerization due to the relatively higher rate of polymer growth in that region. The resulting $N'_{HO,avg}$ is, therefore, lower in sickle cells when $(P_{O_2})_w = 10$ Torr. These effects become more pronounced for higher values of $(P_{O_2})_w$.

The situation where $(P_{O_2})_w = 5$ Torr is an intermediate case where the influence of polymerization on deoxygenation kinetics is weak but not as weak as in the 0 Torr case. Although the product $N'_H(0.0085)$ is quite small in Eq. 85, the effect of polymer formation on N'_H doesn't go "totally unnoticed" by the HbO_2 dissociation reaction. Deoxygenation at the cell boundary does slow down in this case but it is not as slow as when the boundary P_{O_2} is 0 Torr. The effect of slower diffusion toward the cell wall is much more prominent than that of slower deoxygenation and, consequently, the lowering of $N'_{HO}(x' = 1)$ is more pronounced than for the 0 Torr case. This results in a lower spatially averaged concentration of oxyhemoglobin S.

To sum up things, the main reason for the anomaly in Fig. 7 is that when $(P_{O_2})_w < 5$ Torr, the effect of polymerization on deoxygenation kinetics in the region of maximum polymerization is undermined by the existence of very low O_2 concentrations. Because it is physiologically unlikely for the boundary P_{O_2} in the microcirculation to be <5 Torr, we can conclude that in vivo polymerization always accelerates oxygen delivery from sickle cells.

A portion of the O_2 unloading curves for a sickle and normal cell with physiological 2,3-DPG concentrations for a boundary P_{O_2} of 20 Torr are plotted in Fig. 8. The

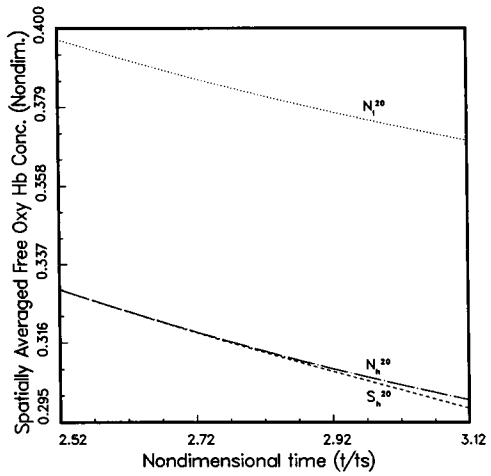

FIGURE 8 Representative oxygen unloading curves for normal (N_l^{20}, N_h^{20}:molar ratios of 1.0 and 1.5, respectively; $[P_{O_2}]_w = 20$ Torr) and sickle cells (S_h^{20}:molar ratio 1.5, $[P_{O_2}]_w = 20$ Torr), during the time interval from t' $(=t/ts) = 2.52$–3.12, expressed in terms of variation of nondimensional, spatially averaged, free oxyhemoglobin concentration, $N'_{HO,avg}$, with t'. $C_{t,i} = 0.34$ g/cc for all three cases. The plasma pH is 7.4. Also, $ts = 0.0688$ s.

unloading curve for a normal cell having the same diphosphoglycerate concentration as the sickle cell is also plotted to show the separate influences of polymer formation and elevated 2,3-DPG/Hb molar ratios on the oxygen delivery process from sickle cells. The effect of elevated molar ratios on the O_2 unloading process seems much more substantial than that of polymerization during the initial part of the polymerization process. The effect of the polymer is, in fact, almost nonexistent for a major part of the unloading process (from $N'_{HO,avg} = 0.95$–0.32). To predict the relative magnitudes of these two effects in the presence of larger amounts of polymer, we studied the trend in the variation of the ratio of "polymer effect"/"DPG effect" with polymer concentration. The "DPG effect" in Fig. 8 is the difference in the magnitudes of $N'_{HO,avg}$ for normal cells with the lower and higher molar ratio (i.e., $N_l^{20} - N_h^{20}$); the "polymer effect" is the difference in oxyhemoglobin concentrations in normal and sickle cells with the same molar ratio ($N_h^{20} - S_h^{20}$).

Fig. 9 depicts how the relative magnitude of these two effects changes with increasing polymer concentration for different boundary conditions. The 0 Torr curve lies below the X-axis because the polymer slows down the process of oxygen unloading for this case. The slope of the 20 Torr curve indicates a rapid increase in the "polymer effect," with the possibility of this effect becoming rather substantial at higher values of n'_H. However, by the time this effect becomes prominent, the cell would have unloaded most of its oxygen under the influence of the higher intracellular

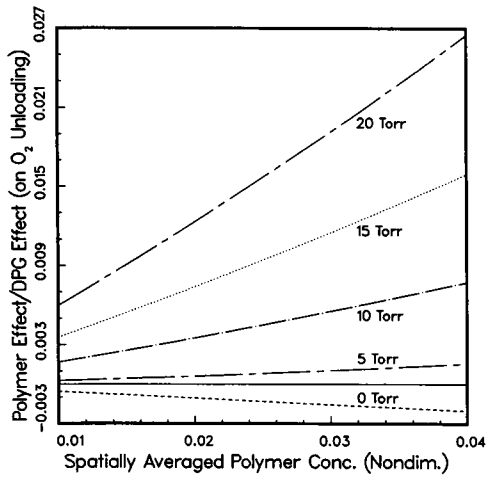

FIGURE 9 The relative effects of polymer formation ($N_h - S_h$) and elevated 2,3-DPG concentrations ($N_l - N_h$) on the oxygen unloading curves for sickle cells (S_h:Molar ratio = 1.5), as compared with normal cells (N_h, N_l:Molar ratios = 1.5 and 1, respectively), for a boundary P_{O_2} of 0, 5, 10, 15, and 20 Torr. $C_{t,i}$ = 0.34 g/cc and pH_e = 7.4

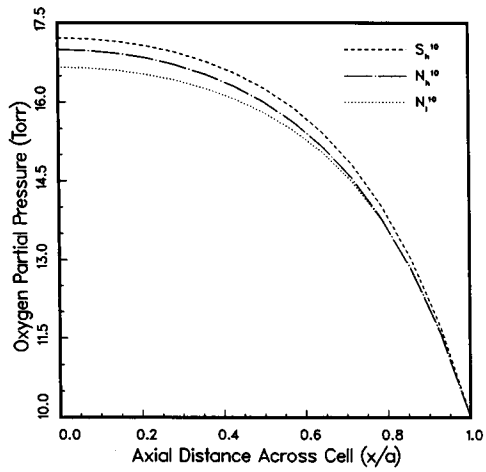

FIGURE 10 Spatial profile of oxygen partial pressure, PO_2 (Torr), during the O_2 unloading process, in the cell half width at t = 0.153 s in normal (N_l^{10}, N_h^{10}:molar ratios of 1 and 1.5, respectively; $[P_{O_2}]_w$ = 10 Torr) and sickle (S_h^{10}:molar ratio = 1.5, $[P_{O_2}]_w$ = 10 Torr) cells with $C_{t,i}$ = 0.34 g/cc. The plasma pH is 7.4; a = 1 μm.

2,3-DPG concentration. ($N'_{HO,avg}$ decreases from 0.95 to 0.298 for $[P_{O_2}]_w$ = 20 Torr when $n'_H \leq 0.04$; the equilibrium saturation is 0.094. The extent of the unloading is even greater for lower values of boundary P_{O_2}). The O_2 unloading curve for sickle erythrocytes seems to be almost biphasic in nature. The accelerated rate of oxygen delivery, for a major part of the unloading process (during the latent period for intracellular polymerization), is due to the higher 2,3-DPG/Hb molar ratio; the influence of the low affinity polymer becomes predominant during the final stages of the process.

Fig. 10 shows the spatial variation of P_{O_2} in sickle and normal red cells with the same HbS density for different 2,3-DPG concentrations. As mentioned earlier, the gradients are steepest at the cell boundary (x' = 1) due to the low oxygen environment outside the cell. Normal cells with the lower 2,3-DPG intraerythrocyte concentration have higher $\tilde{N}'_O$ than their counterparts with the higher 2,3-DPG concentration (due to their higher oxygen affinity). The corresponding P_{O_2}, however, is lower in the former due to the lower values of P_{50} and n for cells with $M.R.$ = 1.0. In the case of sickle cells with the higher molar ratio (S_h), the growing polymer domains near the cell wall interfere with the outward O_2 flux. This obstruction to diffusion overrides the increase in diffusivity of O_2 resulting from a decrease in $[Hb]$. Polymerization, therefore, slows down the diffusion of oxygen in sickle cells. There is also an increase in the rate of deoxygenation caused by the "sink" effect of polymerization. The net effect of slower diffusive fluxes of O_2, a higher rate of oxyhemoglobin dissociation, and, the "concentrating" effect described earlier is an increase in oxygen concentrations in sickle cells, as compared to normal cells with the same 2,3-DPG concentration. The corresponding P_{O_2}'s are, therefore, higher in sickle cells ($S_h > N_h$).

The effect of 2,3-DPG concentration and $(P_{O_2})_w$ on the polymer content in the cell is shown in Fig. 11. The spatial profile of n'_H at t = 0.153 s is plotted for sickle cells with molar ratios of 1 and 1.5, unloading under the same

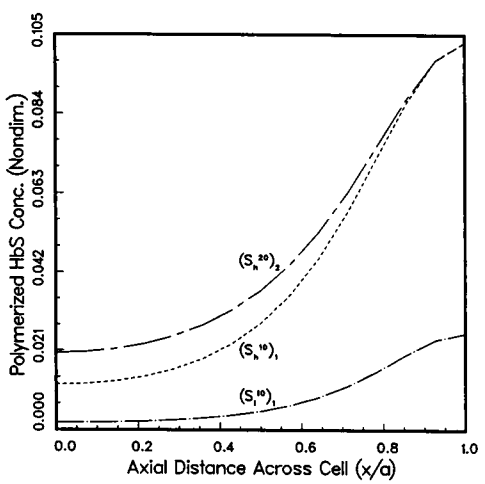

FIGURE 11 Spatial profile of nondimensional, polymerized hemoglobin concentration, n'_H, in the cell half width for three cases: $(S_l^{10})_1$ – molar ratio 1.0, $(P_{O_2})_w$ = 10 Torr, t = 0.153 s; $(S_h^{10})_1$ – molar ratio 1.5, $(P_{O_2})_w$ = 10 Torr, t = 0.153 s; $(S_h^{20})_2$ – molar ratio 1.5, $(P_{O_2})_w$ = 20 Torr, t = 0.215 s. $C_{t,i}$ is 0.34 g/cc and plasma pH is 7.4. Also, a = 1 μm.

boundary condition (P_{O_2} = 10 Torr). The rate of HbO_2 dissociation increases with an increase in 2,3-DPG concentration. This results in a higher rate of formation of deoxy HbS monomers. The HbS solution gets supersaturated at a faster rate and, consequently, there is more polymer everywhere in the cell at any given instant. The concentration gradient of polymerized HbS indicates a higher polymerization rate at the cell boundary than at the center of the cell.

An increase in boundary P_{O_2} slows down the HbO_2 dissociation process and, effectively, the rate of increase of HbS supersaturation. Therefore, for a given 2,3-DPG concentration, a higher $(P_{O_2})_w$ slows down the rate of polymerization everywhere in the cell. In Fig. 11, it takes 0.215 s for $n'_H(x' = 1) = 0.103$ in the cell unloading with a boundary P_{O_2} of 20 Torr; it takes only 0.153 s in the cell having $(P_{O_2})_w$ = 10 Torr. A slower polymerization rate, however, results in higher concentrations of polymer in the interior of the cell as indicated by the spatial profiles of $(S_l^{10})_1$ and $(S_h^{20})_2$ in Fig. 11. This is due to the fact that when Γ'_2 is lower, the deoxy monomer in the interior of the cell has more time to overcome the delay period.

Fig. 12 shows the resultant polymerization curves for sickle cells unloading under different boundary conditions. As discussed earlier, an increase in boundary P_{O_2} slows down the polymerization process. It also tends to increase the net delay time ($t_{cr} + t_d$) for the process. A higher boundary oxygen concentration, however, slows down the oxygen unloading process too. To get an idea of the relative degree of slowing down of these processes, we need to look at the variation of both $N'_{HO,avg}$ and n'_H with time at different values of $(P_{O_2})_w$.

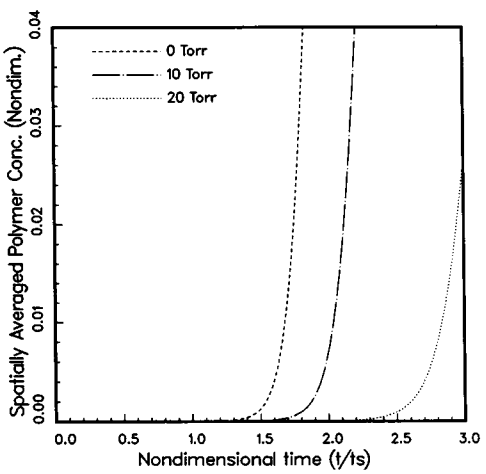

FIGURE 12 The effect of boundary P_{O_2} on the polymerization curves for sickle cells with a hemoglobin density of 0.34 g/cc. The three values of $(P_{O_2})_w$, for a fixed molar ratio of 1.5, are 0 Torr, 10 Torr, and 20 Torr. The plasma pH is 7.4 and ts = 0.0688 s.

The effect of boundary P_{O_2} on oxygen unloading and polymerization is shown cumulatively in Fig. 13. The variation of $n'_{H,avg}/N'_{HO,avg}$ with time is plotted for three values of $N'_{HO,avg}$ (I: 0.5, II: 0.45, and III: 0.4). The boundary P_{O_2}, going left to right along each curve, varies from 0 to 20 Torr. The slope of the curves indicates the presence of larger amounts of polymer at any given oxyhemoglobin concentration for higher values of boundary P_{O_2}. This indicates that a higher boundary oxygen concentration slows down the O_2 delivery process more than it does the gelation of HbS during the initial part of the polymerization process.

Lowering the 2,3-diphosphoglycerate concentration is another way of slowing down both polymerization (see Fig. 11) and oxygen unloading (see Figs. 6 and 8). Fig. 14 depicts the relative effect of lower 2,3-DPG concentration on both processes at a boundary P_{O_2} of 20 Torr. It is clear that lowering the 2,3-DPG/Hb molar ratio slows down oxygen unloading more than it does the polymer formation process.

Another parameter which influences polymerization rates in sickle cells is the hemoglobin density, $C_{t,i}$. The effect of MCHC on polymerization curves is shown in Fig. 15 for a molar ratio of 1.13 and boundary P_{O_2} of 20 Torr. Polymerization curves are plotted for three values of MCHC, 0.35 g/cc (cell 1), 0.34 g/cc (cell 2), and 0.33 g/cc (cell 3). The decrease in the rate of polymerization, corresponding to a 0.01 g/cc decrease in hemoglobin density, is quite significant as indicated by the slopes of the curves at any time $t > 0.06$ s (at t = 0.1 s, the mole

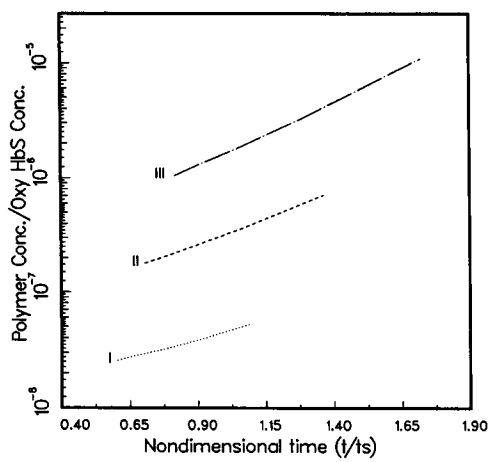

FIGURE 13 The effect of boundary P_{O_2} on the extent of polymerization in sickle cells at a given oxyhemoglobin concentration. This is shown by the variation of $(n'_{H,avg}/N'_{HO,avg})$ with t' $(= t/ts)$ in sickle cells with $C_{t,i}$ = 0.34 g/cc and $M.R.$ = 1.5 for three values of $N'_{HO,avg}$ (I − 0.5; II − 0.45; III − 0.4). $n'_{H,avg}$ varies with t', at a fixed $N'_{HO,avg}$, due to the variation of $(P_{O_2})_w$ from 0 to 20 Torr (*left to right along each curve*). ts = 0.0688 s. pH_e = 7.4.

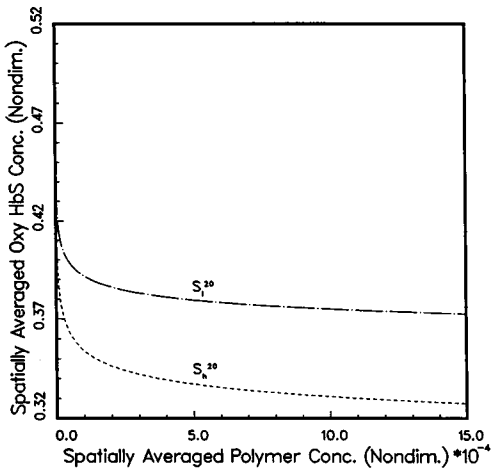

FIGURE 14 The effect of 2,3-DPG concentration on the extent of polymerization in sickle cells at a given oxygen saturation. This is represented by the variation of nondimensional, spatially averaged, free oxyhemoglobin concentration, $N'_{HO,avg}$, as a function of nondimensional, spatially averaged, polymerized HbS concentration, $n'_{H,avg}$, for molar ratios of 1.0 (S_i^{20}) and 1.5 (S_h^{20}) in sickle cells with a hemoglobin density of 0.34 g/cc. The boundary P_{O_2} in both cases is 20 Torr and the plasma pH is 7.4.

fraction of polymer in cell 2 is ~6 times higher than in cell 3; the corresponding ratio for cell 1 is ~50).

Seakins et al. (1973) tried to establish, experimentally, the effect of erythrocyte HbS concentration on the oxygen affinity of blood at 35°C (pH_e = 7.13) and its contribution to the right shift in the O_2-HbS equilibration curve, relative to the contribution from elevated 2,3-DPG/Hb molar ratios. They found that when they increased the HbS concentration from 0.324 g/cc ($C_{t,i}^A$) to 0.362 g/cc ($C_{t,i}^B$), the $(P_{50})_t$ (corresponding to 50% total fractional saturation) increased by ~7.5% despite the decrease in molar ratio from 1.4 to 1.13. This led them to conclude that the intrinsic molecular defect associated with HbS polymerization played an important part in the low oxygen affinity of sickle blood and that HbS concentration had a greater effect on the O_2 affinity than the 2,3-DPG/Hb molar ratio in sickle erythrocytes.

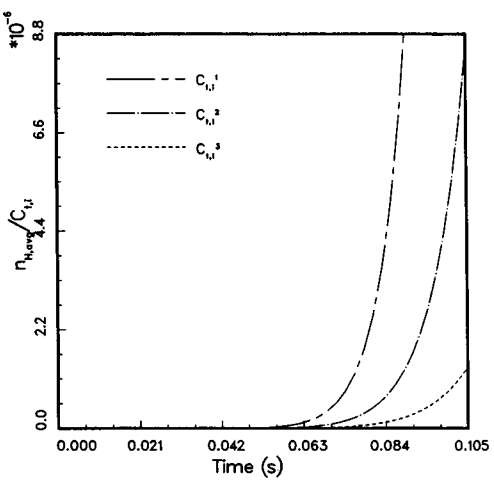

FIGURE 15 The effect of hemoglobin concentration on the extent of polymerization in sickle cells at any given instant. This is represented by the variation of $(n_{H,avg}/C_{t,i})$ with time for sickle cells with molar ratios of 1.13 and hemoglobin densities of 0.35 g/cc ($C_{t,i}^1$), 0.34 g/cc ($C_{t,i}^2$), and 0.33 g/cc ($C_{t,i}^3$). The plasma pH is 7.13 and the boundry P_{O_2}, for both cases, is 20 Torr.

We tried a similar equilibrium analysis at 35°C using our two-phase model to determine theoretically the $(P_{50})_t$'s for these two cases (see Appendix 8). Our analysis also gave us a resultant $(P_{50})_t$ for $C_{t,i}$ = 0.362 g/cc ($M.R.$ = 1.13) which was approximately 8% higher than the $(P_{50})_t$ corresponding to a hemoglobin density of 0.324 g/cc ($M.R.$ = 1.4) although our values were higher than their experimental values. This can be attributed to the fact that the nomogram we use for obtaining the P_{50}'s for normal blood (from Samaja et al., 1981) predicts, in general, higher values than those measured experimentally by Seakins et al. (1973) (Our P_{50} at 37°C, pH_e = 7.13, $M.R.$ = 0.915 was 35.85 Torr; their measured value was 31.4 Torr). On scaling down our P_{50}'s by a factor of 0.876 (=31.4/35.85), we obtained results (given in parentheses in Table 8.1, Appendix 8) that were in excellent agreement with their experimental data. Our $(P_{50})_t$'s were still slightly higher; this is probably because we underestimate oxygen affinities slightly by taking Y_p = 0. To establish the relevance of such equilibrium analysis to the actual O_2 delivery process in the microcirculation, we used our model to simulate the oxygen unloading curves for the two cases for a boundary P_{O_2} of 20 Torr. We also switched the molar ratios for the two values of $C_{t,i}$ to isolate the individual effects of the molar ratio and HbS density on the unloading curve.

Fig. 16 shows the oxygen unloading curves for the four cases. At a fixed value of HbS density, the sickle cell unloads faster when the 2,3-DPG content of the cell is increased. This is due to the effect of the intracellular organic phosphate on deoxygenation kinetics and is in agreement with our equilibrium analysis (see Appendix 8) which predicts higher $(P_{50})_t$'s (and hence lower affinities) at higher 2,3-DPG concentrations for a fixed value of $C_{t,i}$. However, when HbS density is increased and the molar ratio kept constant, the cell seems to unload oxygen at a slower rate despite the prediction of lower O_2 affinity at equilibrium. In fact, the combination of a higher HbS density (0.362 g/cc) and a lower molar ratio (1.13) results in an even slower oxygen delivery process (B1 as compared with A2 in Fig. 16). This "unexpected" trend in

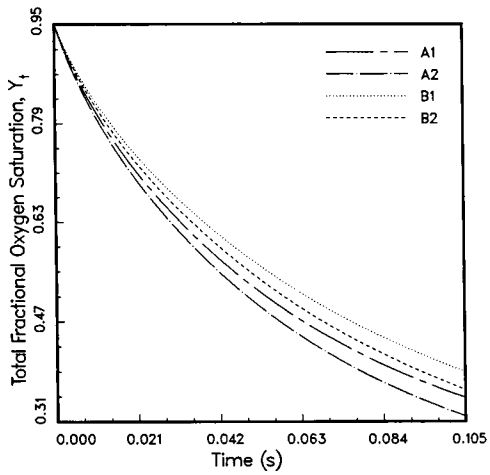

FIGURE 16 The individual effects of hemoglobin density and molar ratio on the oxygen unloading curves in sickle cells, demonstrated by the variation of total fractional oxygen saturation, Y_t ($=N_{HO,avg}/C_{t,i}$), with time for four cases (B1: $C_{t,i} = 0.362$ g/cc, $M.R. = 1.13$; B2: $C_{t,i} = 0.362$ g/cc, $M.R. = 1.4$; A1: $C_{t,i} = 0.324$ g/cc, $M.R. = 1.13$; A2: $C_{t,i} = 0.324$ g/cc, $M.R. = 1.4$). The boundary P_{O_2} is 20 Torr and the plasma pH is 7.13 in all cases.

the oxygen unloading rates can be accounted for by the effect of $C_{t,i}$ on the mechanism of diffusion, a process that is completely ignored in the equilibrium analysis. Increasing the hemoglobin concentration results in lower values of diffusivity (Eqs. 68–71) and, consequently, a slower diffusion process. This decreases the contribution made by the facilitated diffusion of O_2 to the process of unloading, and this effect seems to override the effect of an accelerated rate of formation of the low affinity polymer in the cell. Besides, the existence of nonequilibrium conditions in the sickle erythrocyte during the O_2 unloading result in a lower polymer content as compared with that predicted in the equilibrium model (due to the presence of supersaturated deoxy HbS monomers). The equilibrium predictions of oxygen affinity for higher molar ratios were reasonably accurate because diphosphoglycerate concentrations do not have any significant influence on the diffusion process.

The plots in Fig. 16 clearly indicate that it is not always possible to make accurate predictions about oxygen removal from sickle erythrocytes in the microcirculation based on equilibrium analysis (theoretical or experimental) of the oxygen affinity of the cell. Equilibrium models could probably be useful in predicting the oxy HbS content or polymer concentration in sickle cells from experimentally measured values of P_{O_2} before their entry into the microcirculation or after the oxygen unloading is complete.

SUMMARY

There are three important dynamic processes occurring simultaneously within a sickle erythrocyte during the course of its oxygen delivery in the microcirculation: the oxygen-hemoglobin reactions, deoxyhemoglobin polymerization, and the diffusional processes. A mathematical model, which takes into account the complex interplay among these processes, has been developed to simulate oxygen unloading from sickle erythrocytes which enter the microcirculation polymer-free. It is also used to simulate intracellular polymerization in these cells and study the effects of various parameters, characteristic of blood in sickle cell anemia, on these two processes simultaneously.

This model is as complete as it seems possible to make it at this time, on the basis of our understanding of the data in the literature. The model is applicable as long as local hemoglobin polymerization does not exceed 15% conversion (due to limitations on available polymerization data). This restriction, however, does not significantly undermine the usefulness of this model for the following reasons: (*a*) sickle cells, with a typical MCHC of 0.34 g/cc, unload most of their oxygen before the occurrence of 15% localized polymerization (unloading is 76% complete when the boundary P_{O_2} is 20 Torr; for $[P_{O_2}]_w = 0$ Torr, the extent of the unloading is 89%). (*b*) The model can be used to get more realistic and physiologically relevant estimates of the delay times for intracellular polymerization in the microcirculation. (The significance of these in vivo delay times and their role in the occurence of occlusions in the microvasculature ["microcrises"] has been extensively discussed in the past by Eaton et al., 1976; Noguchi and Schechter, 1981; Mozzarelli et al., 1987; Ferrone, 1989).

The parameters that have a significant influence on oxygen unloading from a sickle cell, are the intracellular 2,3-DPG/Hb molar ratio (as shown in Figs. 6, 8, 11, and 14), the total hemoglobin concentration (Figs. 15 and 16), and, the P_{O_2} of the cell environment (Figs. 11–13). These parameters have a two-part effect on the oxygen unloading process: (*a*) the direct effect these parameters have on oxy HbS dissociation and the free and facilitated diffusion of oxygen in the solution phase (essentially the same effect these parameters would have on oxygen delivery from normal cells), and, (*b*) the indirect effect through their influence on the polymerization process. For example, an increase in MCHC of 0.01 g/cc from 0.33 to 0.34 results in a six-fold increase in the initial rate of polymerization, whereas for a similar increase from 0.34 to 0.35 g/cc, the increase is eight-fold. The formation of HbS polymer has three direct effects: (*a*) physical blockage of diffusional processes in the solution phase by the impermeable,

undiffusing polymer phase, (*b*) alteration of hemoglobin concentration, and, hence, diffusivities of the species and their concentration gradients, in the solution phase, and, (*c*) its effect on chemical reaction kinetics by serving as a "sink" for deoxy HbS from the solution phase and speeding up oxyhemoglobin decomposition. For boundary P_{O_2}'s of physiological significance, the net effect of these processes, within this 15% polymer conversion restriction, is to speed up oxygen unloading from a sickle cell, relative to a normal red cell, at equal total hemoglobin and 2,3-DPG concentrations (Fig. 8).

Sickle red cells, with physiologically higher intracellular 2,3-DPG concentrations, unload oxygen faster than normal red cells. The O_2 unloading curve for sickle erythrocytes is biphasic in nature. The initial (but major) part of the unloading is entirely under the influence of the elevated 2,3-DPG/Hb molar ratio; the latter part of the process is affected by the presence of the low affinity polymer as well (for a sickle cell with $C_{t,i} = 0.34$ g/cc and $M.R. = 1.5$, unloading at a boundary P_{O_2} of 20 Torr, the effect of the polymer is virtually nonexistent during the initial 74% of the desaturation process). These theoretical results indicate that higher rates of oxygen unloading from sickle cells are primarily due to elevated 2,3-diphosphoglycerate concentrations. Our conclusion seems to be in apparent contradiction with the previously established notion (based on experimental data by Seakins et al., 1973 and Winslow, 1978) that formation of the low affinity polymer is the main cause of the right shift in the equilibrium oxygen binding curve for sickle hemoglobin.

This brings us to, perhaps, the most significant conclusion drawn from this model study—*equilibrium data (e.g., $[P_{50}]_t$ data) alone are not a sufficient basis for predicting the time course of oxygen unloading from a sickle red cell.* We have used the model to demonstrate this. We showed that the oxygen unloading rate of a sickle cell, relative to that of a normal red cell with the same MCHC and 2,3-DPG concentration, could be either higher or lower, depending on the boundary oxygen partial pressure (Fig. 7). Equilibrium analysis would have predicted a lower oxygen affinity and, consequently, faster oxygen removal from the sickle cell, as compared with the normal cell, at all boundary P_{O_2}'s. We also analyzed the unloading of oxygen from sickle cells with different MCHC's and 2,3-DPG/Hb molar ratios, using the same values as in the analysis by Seakins et al. (1973). We found that although (*a*) the prediction on relative oxygen affinities for the different cases by our model at equilibrium coincided with the experimental findings by Seakins et al. (1973), (*b*) the actual rate of in vivo oxygen unloading could not be predicted from the oxygen affinities alone. As discussed earlier, one reason for this deviation from simple equilibrium predictions is the role played by diffusion in the facilitation of oxygen removal from the cell, a factor that doesn't show up in the equilibrium analysis. (This is also true for predictions of oxygen unloading from normal cells with different MCHC's.) In addition to this, there is the formation of low affinity polymer and the resulting complex interactions between the three mechanisms of deoxygenation, diffusion, and polymerization that govern O_2 unloading rates. The influence exerted by various parameters such as $(P_{O_2})_w$ on the nature (or degree) of these interactions is not apparent at equilibrium conditions; hence, the result of these interactions, namely the rate of oxygen unloading, cannot be predicted by equilibrium analysis alone.

All model calculations presented here assumed that in the highly oxygenated state, there was no polymer. The intracellular HbS concentration in some cells may be high enough for solubility to be exceeded even at arterial oxygen pressures (Eaton and Hofrichter, 1987). These cells would contain initial amounts of polymerized hemoglobin in equilibrium with the HbS solution prior to oxygen delivery. The effect of this polymer on oxygen unloading would depend on the initial concentration of the polymer, its spatial distribution in the erythrocyte and the influence it exerts on the three governing mechanisms. It is not intuitively obvious how this initial distribution would affect the rate of desaturation (and, effectively, the rate of increase of supersaturation in the solution). Polymerization would begin as soon as the cell enters the microcirculation ($t_{cr} = 0$) and the rate of polymer formation would be enhanced by the presence of heterogenous nucleation sites. The net delay time for intracellular polymerization would probably decrease for this cell (as compared with a polymer-free cell with an MCHC equal to the unpolymerized hemoglobin concentration for the present case); it is doubtful, however, whether the latent period would vanish altogether. It seems quite obvious, at this point, that the effect of initial polymer on in vivo polymerization in sickle cells (where the rate of increase of supersaturation is also a governing factor) is quite different from its effect on polymer formation in deoxy HbS solutions (where t_d is shortened significantly or even eliminated; Hofrichter et al., 1978).

The decrease in delay time could result in an interesting situation in vivo where the rates of all three mechanisms (diffusion, deoxygenation, and polymerization) are comparable in magnitude. (In the present analysis, the rate of polymerization is negligibly small during the initial stages of oxygen unloading when deoxygenation is rapid and the diffusive fluxes are high.) The net effect of initial polymer on oxygen transport could be quite complicated. A theoretical analysis of this situation could give some insight into oxygen delivery from irreversibly sickled cells.

Besides the possibility that polymer is initially present, a number of other controversial effects or poorly characterized effects have not been incorporated in our model.

Among these are morphologic deformation of the cell and its relation to the spatial distribution and concentration of intracellular polymer, the shift of water across the cell membrane during deoxygenation, mechanisms of oxygen incorporation in the deoxyhemoglobin polymer, and the mechanics of 2,3-DPG interaction with polymerized hemoglobin.

APPENDIX 1

Governing equations for formation of critical homogenous and heterogenous nuclei

The activity of the critical nuclei (Eq. A3.11, Ferrone et al., 1985*b*), at 35°C, can be written as

$$(\gamma_{i^*} n^*_{H,i^*}) = (\gamma_{sol} N_{H,sol}) \exp [i^* \ln S - 15.6087 \cdot \ln i^* + 4.5732], \quad \text{(A1.1)}$$

where the size of the critical nucleus, i^*, is

$$i^* = \frac{15.6087}{\ln S}. \quad \text{(A1.2)}$$

Here, the fraction of contacts per monomer present in an infinite polymer (Eq. A3.7, Ferrone et al., 1985*b*), for a homogenous nucleus of size i^*, $\delta(i^*)$, is taken as

$$\delta(i^*) = 1 - \left(\frac{1.34 \ln i^* + 0.8}{i^*}\right). \quad \text{(A1.3)}$$

On substituting the expression for i^* in Eq. A1.1, we get

$$(\gamma_{i^*} n^*_{H,i^*}) = (\gamma_{sol} N_{H,sol}) \cdot \exp [15.6087 \ln (\ln S) - 22.7081]. \quad \text{(A1.4)}$$

The size of the critical heterogenous nucleus (Eq. A3.23, Ferrone et al., 1985*b*), at 35°C is given by

$$j^* = \frac{-2.5419}{(1.2902 - \ln S)} \qquad j^* < 13.2278 \quad \text{(A1.5a)}$$

$$= \frac{16.6087}{\ln S} \qquad j^* > 13.2278. \quad \text{(A1.5b)}$$

In our model, the value of S varies continuously as a function of time. Therefore, it is convenient to rewrite Eqs. A1.5a and b with the criteria based on the value S rather than j^*. The modified equations are of the form

$$j^* = \frac{-2.5419}{(1.2902 - \ln S)} \qquad S > 4.4034 \quad \text{(A1.6a)}$$

$$= \frac{16.6087}{\ln S} \qquad S < 3.5099 \quad \text{(A1.6b)}$$

$$= 13.2278 \quad \text{otherwise.} \quad \text{(A1.6c)}$$

The range of values for S is obtained by equating $j^* = 13.2278$ in Eqs. A1.5a and b.

The concentration of the critical heterogenous nuclei (Eq. A3.21, Ferrone et al., 1985*b*), at 35°C, is given by

$$n^*_{Hj^*} = \phi n_H \exp [j^*(\ln S - 1.2902) - 2.5419 \ln j^* - 11.7067] \qquad j^* < 13.2278 \quad \text{(A1.7a)}$$

$$= \phi n_H \exp [j^* \ln S - 16.6087 \ln j^* + 7.5515] \qquad j^* > 13.2278. \quad \text{(A1.7b)}$$

On rewriting Eqs. A1.7a and b in a manner similar to that for Eqs. A1.5a and b, and using the appropriate expressions for j^*, we get

$$n^*_{Hj^*} = \phi n_H \exp [2.5419 \ln (\ln S - 1.2902) - 11.5362] \qquad S > 4.4034 \quad \text{(A1.8a)}$$

$$= \phi n_H \exp [16.6087 \ln (\ln S) - 22.509] \qquad S < 3.5099 \quad \text{(A1.8b)}$$

$$= \phi n_H \exp [13.2278 \ln S - 35.3375] \qquad \text{otherwise.} \quad \text{(A1.8c)}$$

APPENDIX 2

Activity coefficients

The monomer activity coefficient is a function of the total monomer concentration in the cell which includes the unliganded deoxy HbS monomer and the liganded, nonpolymerizing oxyhemoglobin monomer. It can be computed from the theoretical expression by Ferrone et al., 1985*b*

$$\gamma = f_1(N_H + N_{HO}) = \exp\left[\sum_{n=1}^{6} B_{n+1}(N_H + N_{HO})^n\right], \quad \text{(A2.1)}$$

where $B_2 = 8V$, $B_3 = 15V^2$, $B_4 = 24.48\ V^3$, $B_5 = 35.36V^4$, $B_6 = 47.4V^5$, and $B_7 = 65.9V^6$ with $V = 5.056 \times 10^{-2}\ \text{mM}^{-1}$. N_H and N_{HO} are in millimolar units. Similarly,

$$\gamma_{sol} = f_1(N_{H,sol} + N_{HO}). \quad \text{(A2.2)}$$

The activity coefficient of the activated complex is a function of the total monomer concentration and the size of the critical homogenous nucleus, i^* (given in Appendix 1). It can be expressed as the function $\gamma_{i^*+1} = f_2(N_H, N_{H,sol}, N_{HO})$ where (Ferrone et al., 1985*b*)

$$f_2 = \left(\frac{1}{1-A}\right) \exp\left[\left\{\frac{3A}{1-A}\right\} B^{1/3} + \left\{\frac{3A + 13.5A^2}{(1-A)^2}\right\} B^{2/3} + \left\{\frac{A + A^2 + A^3}{(1-A)^3}\right\} B\right] \quad \text{(A2.3)}$$

with $A = 0.048(N_H + N_{HO})$ and $B = (i^* + 1)/0.5451$. N_H and N_{HO} are in millimolar units. $i^* = i^*(S) = i^*(N_H, N_{H,sol}, N_{HO})$ is given by Eq. A1.2 in Appendix 1.

APPENDIX 3

Transport equations

The fluxes per unit cell volume of the free HbS components are $F_H = v_{eff}\bar{F}_H$ and $F_{HO} = v_{eff}\bar{F}_{HO}$. From Eqs. 19 and 20 and the assumption that

$D_{HO} = D_H$, we get

$$F_{HO} = -v_{eff} D_H \nabla \tilde{N}_{HO} \quad \text{(A3.1)}$$

$$F_H = -v_{eff} D_H \nabla \tilde{N}_H. \quad \text{(A3.2)}$$

For our one-dimensional slab model, the spatial variations are with respect to x; hence, $\nabla = \hat{\imath}\partial/\partial x$. On combining Eqs. 4, 9, A3.1, and A3.2 with Eqs. 2 and 3, we get

$$\frac{\partial N_{HO}}{\partial t} = \frac{\partial}{\partial x}\left[D_H\left(\frac{2v_s}{3 - v_s}\right)\frac{\partial \tilde{N}_{HO}}{\partial x}\right] + K\left[N_H\left(\frac{\tilde{N}_O}{\tilde{N}_{50}}\right)^n - N_{HO}\right] \quad \text{(A3.3)}$$

$$\frac{\partial N_H}{\partial t} = \frac{\partial}{\partial x}\left[D_H\left(\frac{2v_s}{3 - v_s}\right)\frac{\partial \tilde{N}_H}{\partial x}\right] - K\left[N_H\left(\frac{\tilde{N}_O}{\tilde{N}_{50}}\right)^n - N_{HO}\right] - \Gamma_2. \quad \text{(A3.4)}$$

The transport equation for $\tilde{N}_O$ (Eq. 1), expressed in the form of Eq. 6*b*, is

$$\frac{\partial \tilde{N}_O}{\partial t} = -\frac{1}{v_s}\nabla \cdot (v_{eff}\tilde{F}_O) - \tilde{\Gamma}_1 - \frac{\tilde{N}_O}{v_s}\frac{\partial v_s}{\partial t}. \quad \text{(A3.5)}$$

The polymer concentration in the cell, n_H, can be written as

$$n_H = v_p C_p = (1 - v_s) C_p, \quad \text{(A3.6)}$$

where C_p is the polymer density (=constant). Therefore,

$$\frac{\partial n_H}{\partial t} = \Gamma_2 = -\frac{\partial v_s}{\partial t} C_p. \quad \text{(A3.6)}$$

On expressing $\tilde{\Gamma}_1$ as Γ_1/v_s and combining Eqs. 4, 9, 18, A3.5, and A3.6, we get

$$\frac{\partial \tilde{N}_O}{\partial t} = \frac{1}{v_s}\frac{\partial}{\partial x}\left[D_O\left(\frac{2v_s}{3 - v_s}\right)\frac{\partial \tilde{N}_O}{\partial x}\right] - \frac{K}{v_s}\left[N_H\left(\frac{\tilde{N}_O}{\tilde{N}_{50}}\right)^n - N_{HO}\right] + \frac{\tilde{N}_O}{v_s}\frac{\Gamma_2}{C_p}. \quad \text{(A3.7)}$$

APPENDIX 4

Solution fractional oxygen saturation

The solution fractional oxygen saturation, Y_s, can be determined from the mass balance Eqs. 50–52. These equations can be combined to obtain

$$C'_t = v_{sol} C'_{sol} + \left(1 - v_{sol} - \frac{n'_H}{C'_p}\right) C'_H + n'_H, \quad \text{(A4.1)}$$

where $n'_H = v_p C'_p$. Eq. A4.1 can be rewritten as

$$v_{sol} = \frac{C'_p(C'_t - n'_H) - C'_H(C'_p - n'_H)}{C'_p(C'_{sol} - C'_H)}. \quad \text{(A4.2)}$$

On substituting Eq. A4.2 in Eq. 53, we get

$$Y_s = \left\{\frac{N'_{HO} C'_p}{C'_p(C'_t - n'_H) - C'_H(C'_p - n'_H)}\right\}\left(\frac{C'_{sol} - C'_H}{C'_{sol}}\right) \quad \text{(A4.3a)}$$

$$= Q\left(\frac{C'_{sol} - C'_H}{C'_{sol}}\right), \quad \text{(A4.3b)}$$

where Q is independent of Y_s. Eq. A4.3b can be rearranged after expressing C'_{sol} as a fifth-order polynomial function of Y_s (Eq. 47) to obtain a sixth-order polynomial of the form

$$Q(C'_H - e'_1) + (e'_1 - Qe'_2) Y_s + (e'_2 - Qe'_3) Y_s^2 + (e'_3 - Qe'_4) Y_s^3 + (e'_4 - Qe'_5) Y_s^4 + (e'_5 - Qe'_6) Y_s^5 + e'_6 Y_s^6 = 0. \quad \text{(A4.4)}$$

This polynomial has four complex and two real roots (one positive and one negative). Y_s obviously corresponds to the real, positive root.

APPENDIX 5

Hemoglobin and oxygen diffusivity

Spaan et al. (1980) presented experimental data on the variation of hemoglobin diffusivity, D_H, with solution hemoglobin concentration ($[Hb]$) at 25°C. We obtained a good fit to their experimental data with the empirical function:

$$D_H = (14.032 - 95.148[Hb] + 262.78\,[Hb]^2 - 280.08[Hb]^3) \times 10^{-7}\ \text{cm}^2/\text{s}, \quad \text{(A5.1)}$$

where $[Hb]$ is in g/cc solution. The temperature correction is made using a temperature coefficient of 3.3%/°C (valid from 25° to 35°C) given by Keller et al. (1971).

A compilation of the data available on the diffusion coefficient of oxygen in hemoglobin solutions at 25°C was presented by Kreuzer (1970). We obtained an empirical relationship between oxygen diffusivity and solution hemoglobin concentration from his compiled data by curve fitting:

$$D_O = (2.0719 - 4.5056[Hb] - 0.3107[Hb]^2 + 5.1794[Hb]^3) \times 10^{-5}\ \text{cm}^2/\text{s}. \quad \text{(A5.2)}$$

The solution hemoglobin concentration is in g/cc solution.

A temperature correction factor of 1.3 has been used by Clark et al. (1985) to get D_O at 37°C from its corresponding value at 25°C. This would correspond to an approximate value of 2.2%/°C for the temperature coefficient (assuming it remains constant between 25° and 35°C). We used the above value for the temperature coefficient to get D_O at 35°C.

APPENDIX 6

Kinetic parameters

Samaja et al. (1981) have given equations, based on the fitting of an empirical relationship to their data points, which allow an estimation of P_{50} at 37°C at any given molar ratio (within the range 0.3–2.5), pH_e (range 6.9–7.6) and P_{CO_2} (range 20–90 Torr). For P_{CO_2} = 40 Torr, we

can rewrite their Eq. B5 as

$$\log P_{50} = (pH_e - 7.0)\{-5.589 \times 10^{-3} G - 0.3617\} + 0.3088G + 1.6134, \quad \text{(A6.1)}$$

where $G = \log (M.R.)$. At $pH_e = 7.4$, for $T = 37°C$, we get

$$P_{50} = 29.42 \text{ Torr} \quad M.R. = 1 \quad \text{(A6.2a)}$$

$$= 33.32 \text{ Torr} \quad M.R. = 1.5. \quad \text{(A6.2b)}$$

The temperature correction factor, from Kelman and Nunn (1966), is

$$C.F. = 10^{[0.024(T-37)]}, \quad \text{(A6.3)}$$

where T is in degree Centigrade. On multiplying the P_{50}'s in Eq. A6.2*a* and *b* by this correction factor for $T = 35°C$, we get

$$P_{50} = 26.34 \text{ Torr} \quad M.R. = 1 \quad \text{(A6.4a)}$$

$$= 29.84 \text{ Torr} \quad M.R. = 1.5. \quad \text{(A6.4b)}$$

The dissociation rate constant, K, is sensitive to temperature, solution pH (pH_i in our model), and the 2,3-DPG concentration (molar ratio). Due to lack of sufficient literature/data published on the variation of K with pH_i and $M.R.$, we had to use a crude method to get approximate values of the kinetic parameter. K was estimated using the data from Salhany et al. (1970) and Bauer et al. (1973). We outline a sample estimation of K at $pH_i = 7.22$ and $M.R. = 1$ for $T = 35°C$.

Salhany et al. (1970) have given the variation of K with solution pH for a stripped Hb solution ($M.R. = 0$) and a Hb solution with $M.R. = 2$ at 24°C. The approximate values of K at the two molar ratios (0 and 2), corresponding to a pH of 7.22, are 35.6 s^{-1} and 42.6 s^{-1}, respectively. A similar plot of K vs. pH is given by Bauer et al. (1973) at 37°C for molar ratios of 0 and 4.9. At $pH_i = 7.22$, K is ~193.7 s^{-1} for $M.R. = 0$ and 243.9 s^{-1} for $M.R. = 4.9$.

Salhany et al. (1970) have also plotted the variation of K with 2,3-DPG concentration for a fixed hemoglobin concentration ($[Hb] = 0.05$ mM), solution pH ($pH_i = 7.0$) and temperature (24°C), which is, effectively, the variation of K with $M.R.$ (range 0–10). In their plot, K varies almost linearly with $M.R.$ in the range 0–2 and the actual value of K for $M.R. = 1$ is only ~1% higher than that obtained by linear interpolation between $M.R. = 0$ and 2. This variation is nonlinear beyond a molar ratio of 2, the value of K for $M.R. = 1$ being ~5% higher than that from linear interpolation between $M.R. = 0$ and 4.9. We somewhat arbitrarily assume that the shape of the curve is invariant with temperature and pH. In other words, we assume that K, at $pH_i = 7.22$, is approximately 1% ($T = 24°C$) and 5% ($T = 37°C$) higher than the corresponding linear interpolation values between molar ratios 0 and 2, and 0 and 4.9, respectively. This gives us, at $pH_i = 7.22$, $M.R. = 1$,

$$K = 39.49 \text{ s}^{-1} \quad T = 24°C \quad \text{(A6.5a)}$$

$$K = 214.14 \text{ s}^{-1} \quad T = 37°C. \quad \text{(A6.5b)}$$

The value of K at 35°C can be estimated from an Arrhenius plot ($\log_{10} K$ vs. reciprocal of absolute temperature) of the above values. Because $\log_{10} K$ varies linearly with $1/T$ (absolute), we get

$$K = 167 \text{ s}^{-1} \quad (pH_i = 7.22; M.R. = 1; T = 35°C). \quad \text{(A6.6)}$$

We use the same procedure to get K at the higher molar ratio. Thus,

$$K = 179 \text{ s}^{-1} \quad (pH_i = 7.22; M.R. = 1.5; T = 35°C). \quad \text{(A6.7)}$$

APPENDIX 7

Spatial partial derivatives at the boundary nodes

The first and second order spatial derivatives of the concentration of a species "k" (O_2, oxy HbS or deoxy HbS) at the cell center and wall, expressed in a centered difference form, at any instant t', are

$$\left.\frac{\partial \tilde{N}'_k}{\partial x'}\right|_{x'=0} = \frac{\tilde{N}'_k(\Delta x', t') - \tilde{N}'_k(-\Delta x', t')}{2\Delta x'} \quad \text{(A7.1)}$$

$$\left.\frac{\partial^2 \tilde{N}'_k}{\partial (x')^2}\right|_{x'=0} = \frac{\tilde{N}'_k(\Delta x', t') + \tilde{N}'_k(-\Delta x', t') - 2\tilde{N}'_k(0, t')}{(\Delta x')^2} \quad \text{(A7.2)}$$

$$\left.\frac{\partial \tilde{N}'_k}{\partial x'}\right|_{x'=1} = \frac{\tilde{N}'_k(1 + \Delta x', t') - \tilde{N}'_k(1 - \Delta x', t')}{2\Delta x'} \quad \text{(A7.3)}$$

$$\left.\frac{\partial^2 \tilde{N}'_k}{\partial (x')^2}\right|_{x'=1} = \frac{\tilde{N}'_k(1 + \Delta x', t') + \tilde{N}'_k(1 - \Delta x', t') - 2\tilde{N}'_k(1, t')}{(\Delta x')^2}, \quad \text{(A7.4)}$$

respectively. Fictitious node values, $\tilde{N}'_k(-\Delta x', t')$ and $\tilde{N}'_k(1 + \Delta x', t')$, are used to make the finite difference forms of the partial derivatives accurate to the second order (truncation error of the order $[\Delta x']^2$). Because all first-order spatial derivatives have the value 0 at the cell center (Eqs. 36–38) and because the first-order spatial derivatives of oxy and deoxy HbS concentration are equal to zero at the cell wall (Eqs. 39 and 40), we get, from Eqs. A7.1 and A7.3,

$$\tilde{N}'_k(-\Delta x', t') = \tilde{N}'_k(\Delta x', t') \quad \text{(A7.5)}$$

$$\tilde{N}'_k(1 + \Delta x', t') = \tilde{N}'_k(1 - \Delta x', t'). \quad \text{(A7.6)}$$

On substituting these values in Eqs. A7.2 and A7.4, we get

$$\left.\frac{\partial^2 \tilde{N}'_k}{\partial (x')^2}\right|_{x'=0} = \frac{2[\tilde{N}'_k(\Delta x', t') - \tilde{N}'_k(0, t')]}{(\Delta x')^2} \quad \text{(A7.7)}$$

$$\left.\frac{\partial^2 \tilde{N}'_k}{\partial (x')^2}\right|_{x'=1} = \frac{2[\tilde{N}'_k(1 - \Delta x', t') - \tilde{N}'_k(1, t')]}{(\Delta x')^2}. \quad \text{(A7.8)}$$

Eqs. A7.7 and A7.8 are used to determine the second-order spatial derivatives of oxy and deoxyhemoglobin concentrations at $x' = 0$ and 1 and of oxygen concentration at $x' = 0$. The value of $\partial^2 \tilde{N}'_O/\partial (x')^2$ at $x' = 1$ is redundant since the boundary oxygen partial pressure has a fixed value and the mass transport equation for $\tilde{N}'_O$ isn't solved for that node.

APPENDIX 8

Equilibrium analysis for oxygen affinity

The total fractional oxygen saturation of HbS, from mass conservation of oxygen, is given by (Sunshine et al., 1982)

$$Y_t = x_s Y_s + x_p Y_p, \quad \text{(A8.1)}$$

where x_p and x_s are mole fractions of the polymer phase and solution phase hemoglobin. Because there is no oxygen in the polymer in our model, the polymer phase fractional oxygen saturation, Y_p, is equal to zero. Mass conservation of hemoglobin requires that

$$x_p = 1 - x_s \tag{A8.2}$$

$$= \frac{C_p(C_t - C_{sol})}{C_t(C_p - C_{sol})} \quad \text{(from Ross } et\ al.\text{, 1977).} \tag{A8.3}$$

We use the Hill equation to get the solution fractional oxygen saturation:

$$Y_s = \frac{(P_{O_2}/P_{50})^n}{1 + (P_{O_2}/P_{50})^n}. \tag{A8.4}$$

Because this equilibrium analysis is done to compare our theoretical results with those obtained experimentally by Seakins et al. (1973), we used their values of plasma pH, molar ratio and hemoglobin concentration. Hence, in this analysis, we use a molar ratio of 0.915 (14.3 μmol/g HbS) to represent normal blood. From A6.1, at $T = 37°C$ and $pH_e = 7.13$, we get

$$P_{50} = 35.85 \text{ Torr} \quad M.R. = 0.915. \tag{A8.5}$$

Applying the temperature correction (Eq. A6.3) for $T = 35°C$, we get

$$P_{50} = 32.1 \text{ Torr} \quad M.R. = 0.915 \tag{A8.6}$$

The corresponding Hill coefficient, from Winslow et al. (1983), is 2.62. The P_{50} at molar ratios of 1.13 and 1.4 and the corresponding Hill coefficient ($n = 2.64$) are given earlier (Eqs. 72 and 73). For our convenience, we rewrite. Eq. 47 as

$$C_{sol} = 0.161 + 0.2901\ Y_s - 1.9235\ Y_s^2 + 6.2436 \cdot Y_s^3 - 8.264\ Y_s^4 + 3.9754\ Y_s^5, \tag{A8.7}$$

where the solubility is in grams per cubic centimeter. The polymer density is 0.69 g/cc.

TABLE 8.1 Effect of C_t and *M.R.* on $(P_{50})_t$

Cases ($pH_e = 7.13$)	$(P_{50})_t$ [*Torr*] Our model ($T = 35°C$)	$(P_{50})_t$ [*Torr*] Seakins et al., 1973 ($T = 37°C$)
(*a*) Normal (*M.R.* = 0.915)	32.1 (28.12)*	31.4
(*b*) Sickle (*M.R.* = 0.915, $C_t = 0.324\ g/cc$)	48.2	—
(*c*) Sickle (*M.R.* = 0.915, $C_t = 0.362\ g/cc$)	55.57	—
(*d*) Sickle (*M.R.* = 1.4, $C_t = 0.324\ g/cc$)	54.77 (47.98)*	46.3
(*e*) Sickle (*M.R.* = 1.13, $C_t = 0.362\ g/cc$)	59.30 (51.94)*	49.8

*Values obtained when our P'_{50}s are scaled down by a factor such that our value for normal blood (*M.R.* = 0.915) at 37°C coincides with the experimental value from Seakins et al. (1973).

We used Eqs. A8.1–A8.4 and A8.7 along with the corresponding values of P_{50} and n to get $Y_t = Y_t(P_{O_2})$ for fixed values of C_t and the 2,3-DPG/Hb molar ratio. The P_{O_2} at which $Y_t = 0.5$ is the $(P_{50})_t$ of the equilibrium oxygen dissociation curve for the given sample. Our theoretical results are listed and compared with the experimental results of Seakins et al. (1973) below in Table 8.1

This research was supported by National Institutes of Health grants HL 31608 and HL 37205 from the National Heart, Lung, and Blood Institute. Computations were done at the National Cornell Supercomputer Facility, a resource of the Center for Theory and Simulation in Science and Engineering (Theory Center), which receives major funding from the National Science Foundation and IBM Corporation, with additional support from New York State and members of the Corporate Research Institute.

Received for publication 19 March 1990 and in final form 18 June 1990.

REFERENCES

Arnone, A. 1972. X-Ray diffraction study of binding of 2,3-diphosphoglycerate to human deoxyhaemoglobin. *Nature (Lond.).* 273:146–149.

Basak, S., F. A. Ferrone, and J. T. Wang. 1988. Kinetics of domain formation by sickle hemoglobin polymers. *Biophys. J.* 54:829–843.

Bauer, C., R. A. Klocke, D. Kamp, and R. E. Forster. 1973. Effect of 2,3-diphosphoglycerate and H^+ on the reaction of O_2 and hemoglobin. *Am. J. Physiol.* 224:838–847.

Baxley, P. T., and J. D. Hellums, 1983. A simple model for simulation of oxygen transport in the microcirculation. *Ann. Biomed. Eng.* 11:401–416.

Behe, M. J., and S. W. Englander. 1978. Sickle hemoglobin gelation: reaction order and critical nucleus size. *Biophys. J.* 23:129–145.

Bishop, M. F., and F. A. Ferrone. 1984. Kinetics of nucleation controlled polymerization: a perturbation treatment for use with a secondary pathway. *Biophys. J.* 46:631–644.

Charache, S., S. Grisolia, A. J. Fiedler, and A. E. Hellegers. 1970. Effect of 2,3-diphosphoglycerate on oxygen affinity of blood in sickle-cell anemia. *J. Clin. Invest.* 49:806–812.

Chien, S., S. Usami, and J. F. Bertles. 1970. Abnormal rheology of oxygenated blood in sickle cell anemia. *J. Clin. Invest.* 49:623–634.

Clark. A. Jr., W. J. Federspiel, P. A. A. Clark, and G. R. Cokelet. 1985. Oxygen delivery from red cells. *Biophys. J.* 47:171–181.

Colleta, M., J. Hofrichter, F. A. Ferrone, and W. A. Eaton. 1982. Kinetics of sickle haemoglobin polymerization in single red cells. *Nature (Lond.).* 300:194–197.

Crank, J. 1975. The Mathematics of Diffusion. Oxford Clarendon Press, London. 414 pp.

Eaton, W. A., and J. Hofrichter. 1978. Successes and failures of a simple nucleation theory for sickle hemoglobin gelation. *In* Biochemical and Clinical Aspects of Hemoglobin Abnormalities. W. Caughey, editor. Academic Press, New York. 443–457.

Eaton, W. A., and J. Hofrichter. 1987. Hemoglobin S gelation and sickle cell disease. *Blood.* 70:1245–1266.

Eaton, W. A., J. Hofrichter, and P. D. Ross. 1976. Delay time of gelation: a possible determinant of clinical severity in sickle cell disease. *Blood.* 47:621–627.

Federspiel, W. J. 1983. Engineering analysis of two blood transport problems. Ph.D. thesis, University of Rochester, Rochester, NY. 326 pp.

Ferrone, F. A. 1989. Kinetic models and the pathophysiology of sickle cell disease. *In* Annals of New York Academy of Science, 565: Sickle Cell Disease. C. F. Whitten and J. F. Bertles, editors. 63–74.

Ferrone, F. A., J. Hofrichter, H. R. Sunshine, and W. A. Eaton. 1980. Kinetic studies on photolysis-induced gelation of sickle cell hemoglobin suggests a new mechanism. *Biophys. J.* 32:361–380.

Ferrone, F. A., J. Hofrichter, and W. A. Eaton. 1985*a*. Kinetics of sickle hemoglobin polymerization; I. Studies using temperature jump and laser photolysis techniques. *J. Mol. Biol.* 183:591–610.

Ferrone, F. A., J. Hofrichter, and W. A. Eaton. 1985*b*. Kinetics of sickle hemoglobin polymerization; II. A double nucleation mechanism. *J. Mol. Biol.* 183:611–631.

Goldberg, M. A., A. T. Lalos, and H. F. Bunn. 1981. The effect of erythrocyte membrane preparations on the polymerization of sickle hemoglobin. *J. Biol. Chem.* 256(1):193–197.

Goldberg, M. A., A. T. Lalos, B. Himmelstein, and H. F. Bunn. 1982. Effects of red cell membrane on the polymerization of sickle hemoglobin. *Blood Cells.* 8:237–241.

Hofrichter, J., P. D. Ross, and W. A. Eaton. 1976. A physical description of hemoglobin S gelation. *In* Proceedings of the Symposium on Molecular and Cellular Aspects of Sickle Cell Disease. J. H. Hercules, G. L. Cottam, M. R. Waterman, and A. N. Schechter, editors. DHEW Publication No. 76–1007:185–222.

Hofrichter, J., J. S. Gethner, and W. A. Eaton. 1978. Mechanism of sickle cell hemoglobin gelation. *Biophys. J.* 24:20a (*Abstr.*)

Jensen, M., H. F. Bunn, G. Halikas, Y. W. Kan, and D. G. Nathan. 1973. Effects of cyanate and 2,3-diphosphoglycerate on sickling: relationship to oxygenation. *J. Clin. Invest.* 52:2542–2547.

Keller, K. H., E. R. Canales, and S. I. Yum. 1971. Tracer and mutual diffusion coefficients of proteins. *J. Phys. Chem.* 75:379–387.

Kelman, G. R., and J. F. Nunn. 1966. Nomograms for correction of blood P_{O_2}, P_{CO_2}, pH and base excess for time and temperature. *J. Appl. Physiol.* 21:1484–1490.

Kreuzer, F. 1970. Facilitated diffusion of oxygen and its possible significance; a review. *Respir. Physiol.* 9:1–30.

Kutchai, H. 1970. Numerical study of oxygen uptake by layers of hemoglobin solution. *Respir. Physiol.* 10:273–284.

Lemon, D. D., P. K. Nair, E. J. Boland, J. S. Olson, and J. D. Hellums. 1987. Physiological factors affecting oxygen transport by hemoglobin in an in-vitro capillary system. *J. Appl. Physiol.* 62:798–806.

Linke, W. F. 1965. Solubilities. Vol. II. 4th ed. American Chemical Society, Washington, DC. 1914 pp.

MacDonald, R. 1977. Red cell 2,3-diphosphoglycerate and oxygen affinity. *Anaesthesia.* 32:544–553.

Minton, A. P. 1974. A thermodynamic model for gelation of sickle hemoglobin. *J. Mol. Biol.* 82:483–498.

Minton, A. P. 1975. Thermodynamic analysis of the chemical inhibition of sickle hemoglobin gelation. *J. Mol. Biol.* 95:289–307.

Minton, A. P. 1976. Relations between oxygen saturation and aggregation of sickle cell hemoglobin. *J. Mol. Biol.* 100:519–542.

Minton, A. P. 1977. Non-ideality and the thermodynamics of sickle hemoglobin gelation. *J. Mol. Biol.* 110:89–103.

Minton, A. P. 1983. The effect of volume occupancy upon the thermodynamic activity of proteins: Some biochemical consequences. *Mol. Cell. Biochem.* 55:119–140.

Moll, W. 1969. The influence of hemoglobin diffusion on oxygen uptake and release by red cells. *Respir. Physiol.* 6:1–15.

Monod, J., J. Wyman, and J. P. Changeux. 1965. On the nature of allosteric transitions: a plausible model. *J. Mol. Biol.* 12:88–118.

Mozzarelli, A., J. Hofrichter, and W. A. Eaton. 1987. Delay time of hemoglobin S polymerization prevents most cells from sickling in vivo. *Science (Wash. DC).* 237:500–506.

Noguchi, C. T., and A. N. Schechter. 1981. The intracellular polymerization of sickle hemoglobin and its relevance to sickle cell disease. *Blood.* 58:1057–1068.

Noguchi, C. T., D. A. Torchia, and A. N. Schechter. 1980. Determination of deoxyhemoglobin S polymer in sickle erythrocytes upon deoxygenation. *Proc. Natl. Acad. Sci. USA.* 77:5487–5491.

Pennelly, R. R., and R. W. Noble. 1978. Functional identity of hemoglobins S and A in the absence of polymerization. *In* Biochemical and Clinical Aspects of Hemoglobin Abnormalities. W. Caughey, editor. Academic Press, New York. 401–411.

Poillon, W. N., B. C. Kim, E. V. Welty, and J. A. Walder. 1986. The effect of 2,3-diphosphoglycerate on the solubility of deoxyhemoglobin *S. Arch. Biochem. Biophys.* 249(2):301–305.

Ross, P. D., J. Hofrichter, and W. A. Eaton. 1977. Thermodynamics of gelation of sickle cell deoxyhemoglobin. *J. Mol. Biol.* 112:111–134.

Salhany, J. M., R. S. Elliot, and H. Mizukami. 1970. The effects of 2,3-diphosphoglycerate on the kinetics of deoxygenation of human hemoglobin. *Biochem. Biophys. Res. Commun.* 39:1052–1057.

Samaja, M., and R. M. Winslow. 1979. The separate effects of H^+ and 2,3-DPG on the oxygen equilibrium curve of human blood. *Br. J. Haematol.* 41:373–381.

Samaja, M., A. Mosca, M. Luzzana, L. Rossi-Bernardi, and R. M. Winslow. 1981. Equations and nomogram for the relationship of human blood P_{50} to 2,3-diphosphoglycerate, CO_2 and H^+. *Clin. Chem.* 27(11):1856–1861.

Seakins, M., W. N. Gibbs, P. F. Milner, and J. F. Bertles. 1973. Erythrocyte HbS concentration—an important factor in the low oxygen affinity of blood in sickle cell anemia. *J. Clin. Invest.* 52:422–432.

Sheth, B. V. 1979. Oxygen transport in hemoglobin solutions. Applications in the microcirculation. Master's thesis. Rice University, Houston, TX. pp 112.

Sheth, B. V., and J. D. Hellums. 1980. Transient oxygen transport in hemoglobin layers under conditions of the microcirculation. *Ann. Biomed. Eng.* 8:183–196.

Singer, K., and L. Singer. 1953. The gelling phenomenon of sickle cell hemoglobin: its biological and diagnostic significance. *Blood.* 8:1008–1023.

Spaan, J. A. E., F. Kreuzer, and F. K. van Wely. 1980. Diffusion coefficients of oxygen and hemoglobin as obtained simultaneously from photometric determination of the oxygenation of layers of hemoglobin solutions. *Pfluegers Arch. Eur. J. Physiol.* 384:241–251.

Stathopoulous, N. A., P. K. Nair, and J. D. Hellums. 1987. Oxygen transport studies of normal and sickle red cell suspensions in artificial capillaries. *Microvasc. Res.* 34:200–210.

Sunshine, H. R., J. Hofrichter, and W. A. Eaton. 1979. Gelation of sickle cell hemoglobin in mixtures with normal adult and fetal hemoglobins. *J. Mol. Biol.* 133:435–467.

Sunshine, H. R., J. Hofrichter, F. A. Ferrone, and W. A. Eaton. 1982. Oxygen binding by sickle cell hemoglobin polymers. *J. Mol. Biol.* 158:251–273.

Winslow, R. M. 1978. Hemoglobin interactions and whole blood oxygen equilibrium curves in sickling disorders. *In* Biochemical and Clinical Aspects of Hemoglobin Abnormalities. W. Caughey, editor. Academic Press, Inc., New York. 369–388.

Winslow, R. M., M. Samaja, N. J. Winslow, L. Rossi-Bernardi, and R. J. Shrager. 1983. Simulation of continuous blood O_2 equilibrium curve over physiological pH, DPG, and P_{CO_2} range. *J. Appl. Physiol.* 54(2):524–529.

Zarkowsky, H. S., and R. M. Hochmuth. 1977. Experimentally induced alterations in the kinetics of erythrocyte sickling. *Blood Cells.* 3:305–312.